TN-96

EFFECT OF INCREASE IN GREENHOUSE GASES ON RADIATION, ALBEDO AND EVAPORATION

NATIONAL INSTITUTE OF HYDROLOGY
JAL VIGYAN BHAWAN
ROORKEE-247667

1992-93

PREFACE

Concentrations of several gases viz. carbon dioxide, methane, nitrous oxide, chlorofluorocarbons in the atmosphere have significantly increased since the dawn of the industrial era. The observed built up of the gaseous pollutants has enhanced the so called greenhouse effect and hence increased the radiative heating of the globe. The perturbations in the radiative balance of the earth - atmosphere system have lead to global warming. This is expected to have profound impact on meteorological and hence hydrological parameters. The understandig of alterations in the radiation balance due to increase in greenhouse gas concentrations is a prerequisite to understand the impact of global warming on meteorological and hydrological parameters

The National Institute of Hydrology established the Atmospheric Land Surface Modelling Division with the major objective of carrying out studies and research on coupled atmosphere land surface processes. In the present report an attempt has been made to review the studies carried out on effect of increase in greenhouse gases on radiation, albedo and evaporation.

The report has been prepared by Dr. Divya, Scientist 'B' in Atmospheric Land Surface Modelling Division and it has been typed by Shri Rajneesh Kumar Goyal.

Satish Chandra

(Satish Chandra)
Director

CONTENTS

		Page No.
	LIST OF FIGURES	i
	LIST OF TABLES	iv
	ABSTRACT	v
1.0	INTRODUCTION	1
2.0	RADIATION BUDGET OF EARTH ATMOSPHERE SYSTEM	1
	2.1 Radiatively Important Atmospheric Constituents	7
	2.2 Role of Greenhouse Gases in Affecting the Radiation Balance	10
	2.3 Trends of Increase in Greenhouse Gases	18
3.0	ALBEDO - RADIATION CHARACTERISTICS OF UNDERLYING SURFACES	18
4.0	EVAPORATION	25
5.0	INCREASE IN GREENHOUSE GASES AND CLIMATE MODEL IMPLICATIONS	31
	5.1 Radiation and Albedo	31
	5.2 Evaporation	44
6.0	RADIATIVE SIGNAL OF INCREASING CARBON DIOXIDE - EXPERIMENTAL APPROACH	44
7.0	REMARKS	47
	REFERENCES	49

LIST OF FIGURES

Figure No.	Title	Page No.
2.1	Energy flow diagram	3
2.2	Earth's energy budget	4
2.3a	Spectral distribution of the radiations from the sun and the earth	9
2.3b	Atmospheric absorption of the solar radiation by greenhouse gases	9
2.4	Temperature structure of the atmosphere	13
2.5	Contribution of greenhouse gases to net radiative heating rate as a function of altitude	14
2.6	Annual mean radiative budget for the stratosphere	16
2.7	Annual mean radiative budget for the troposphere	16
2.8	Annual mean radiative budget for the earth's surface	17
2.9	Global annual mean solar and long wave flux components	17
2.10	Concentrations of carbon dioxide, methane, nitrous oxide and chlorofluoro carbons	20
3.1	Latitudinal distribution of annual average zonal surface albedo.	24
4.1	Simulation of impact of CO_2 increase on catchment yield in 1973	27
5.1	Latitudinal distribution of the changes	33

in surface heat flux due to a doubling of the CO_2 content

5.2 Latitudinal distribution of the surface albedo for normal and doubled CO_2 concentrations 34

5.3 Changes in upward radiation fluxes at the top of the atmosphere for doubling of CO_2 content 35

5.4 Seasonal variations of hemispheric and global mean values of solar, terrestrial and net radiative fluxes at the top of model atmosphere 37

5.5 Latitudinal distribution of the zonal mean difference in the net incoming solar radiation between $4xCO_2$ and $2xCO_2$ experiment at the top of the model atmosphere 38

5.6 Seasonal variation of the zonal mean differences of various balance component (Wm^{-2}) at the earth's surface between $4xCO_2$ and $2xCO_2$ experiments at (a) Ocean surface at 82°N(b) continental surface at 65°N. 40

5.7 Latitude time distribution of zonal mean difference in net incoming solar radiation at top of the model atmosphere between $4xCO_2$ and $1xCO_2$ experiment (a) continents (b) oceans 41

5.8 Planetary albedo difference between $2xCO_2$ and $1xCO_2$ experiment for (a) Dec-Jan-Feb (b) Jun-Jul-Aug 42

5.9 Sea ice extent (the limit of ice 0.2 m thick) for $1xCO_2$ experiment (solid 45

line) and the $2xCO_2$ case (dashed line). Hatching indicates areas of sea ice retreat between control and $2xCO_2$ (a) DJF, (b) JJA

5.10 Latitudinal distribution of (a) zonal mean precipitation rate and (b) zonal mean evaporation rate in cm/day. 46

LIST OF TABLES

Table No.	Title	Page No.
2.1	Energy budget of the atmosphere	5
2.2	Atmospheric constituents and their volume mixing ratio	8
2.3	Volume mixing ratios of trace gases other than CO_2	11
2.4	Summary of key greenhouse gases affected by human activities	19
3.1	Range of Published surface albedo values for different surface types	22
3.2	Summary of latitudinal distribution of average surface albedo estimates	23
4.1	Climatic and hydrological variables under scenario 0 and scenario 1	29
4.2	Sensitivity of evapotranspiration to climate change and direct effects of CO_2 in a wheat field, a forest and a grassland.	30

ABSTRACT

Concentrations of greenhouse gases in the atmosphere - carbon dioxide, methane, nitrous oxide, chlorofluorocarbons have increased considerably from pre-industrial levels and are increasing at an alarming rate. The direct effect of this increase is the alteration in global radiation balance. The changes in radiative components or the radiative perturbations alter the temperature of the earth-atmosphere system, which in turn affects the wind fields and other climatic parameters. The change in climate has considerable impact on hydrological regime. Hence, the understanding of how the radiation balance is affected by increasing greenhouse gas concentrations, is a pre requisite for impact studies. The present report gives an over view of the radiative energy budget of the earth atmosphere system, the role of greenhouse gases in affecting the radiation balance and the trends of increase of these radiatively active gases. A review has been presented on the global climate model implications for increase in greenhouse gases in relation to radiation, albedo and evaporation.

1.0 INTRODUCTION

The potential climatic effects of the increasing atmospheric carbon dioxide and other trace gas (methane, nitrous oxide, chlorofluoro carbons, ozone) concentrations, as currently projected by numerical models of the climate system, would constitute a major, extended alterations of the climate regime, that may have far reaching impacts on hydrology and water resources. Alterations in spatial and temporal redistribution of regional water resources due to the changes in runoff, soil moisture, evapotranspiration are expected. These would arise due to changes in climatic parameters as radiation, temperature, humidity, precipitation, wind etc. and are a matter of concern to the hydrologists.

The direct effect of changing carbon dioxide and trace gas concentrations is alteration of the global radiation balance. This radiative perturbation in turn alters temperatures, which then alters wind fields and other climatic parameters in a continuing sequence. An initial step in isolating CO_2-induced climate changes would be identification of the radiative purturbation. The changes in solar radiation absorbed by the atmosphere and surface of the earth, albedo of the surface, terrestrial longwave radiation, latent and sensible heat fluxes due to increase in greenhouse gases are to be known for evaluation of CO_2 induced climate changes and its impacts.Climate models have been used as a tool for assessing the changes in various meteorological parameters due to increase in greenhouse gases.

In the present report a review has been carried out on studies related with effects of increase in greenhouse gases on radiation, albedo and evaporation. Role of greenhouse gases in affecting the radiation balance has been presented and the implications of different global climate models in relation to changes in radiation, albedo and evaporation for doubling of carbon dioxide has been focused upon.

2.0 RADIATION BUDGET OF EARTH ATMOSPHERE SYSTEM

To better understand how increases in CO_2 perturb the radiation balance of the atmosphere, it is important to understand the radiation budget of the unperturbed atmosphere first.

Practically all of the atmospheres energy comes from the

sun. Intercepted first by the atmosphere, a small part is directly absorbed, particularly by gases as ozone and water vapour. Some of the energy is reflected back to space by the atmosphere, its clouds and the earth's surface; some of the sun's radiant energy is absorbed by the earth's surface. Transfers of energy between the earth's surface and the atmosphere occur in a variety of ways, such as by radiation, conduction, evaporation and convection. Kinetic energy (air in motion, or wind) results from differences in temperature within the atmosphere. And finally, friction is constantly bleeding some of the energy of motion, converting it to heat. Figure 2.1 shows the energy flow diagram depicting these processes.

Figure 2.2 presents a summary of what happens, on the average, to the solar radiation intercepted by the earth and its atmosphere. Although normally about 50 percent of the earth's surface is covered by clouds, they absorb only about 3 percent of the solar short wave radiation. Approximately 16 percent is absorbed by the gases and dust of the atmosphere, principally by water vapour. This means that a total of 19 percent is absorbed by the atmosphere and its constituents.

The earth's surface absorbs about 51 percent of the solar radiation. Some of it (24 percent) comes directly from the sun; some (22 percent) after reflection by clouds, the rest (5 percent) is received after being scattered by the air. Thus, of the total energy arriving from the sun, 70 percent is absorbed by the earth's surface and atmosphere. The rest, 30 percent is lost to space, having being reflected by the clouds and the earth's surface or scattered by the particles in the air. This average reflectivity, or albedo, of the earth (0.30) represents the fractional part of the incident radiation that is bounced off the earth.

The manner in which the energy budget is balanced and the approximate amounts reflected, scattered, absorbed and re-radiated are shown in Table 2.1. Of the average amount of short wave solar radiation received by the earth and its atmosphere (0.50 $cal/cm^2/min$), 0.35 $cal/cm^2/min$ is absorbed by the atmosphere and the earth. The remainder (0.15 $cal/cm^2/min$) is immediately lost to space by reflection and scattering. After going through the complex exchange processes described in Figs. 2.1 and 2.2, energy which was absorbed is re-radiated again to outer space, thus keeping the budget in balance.

It should be noted that although there is a heat balance

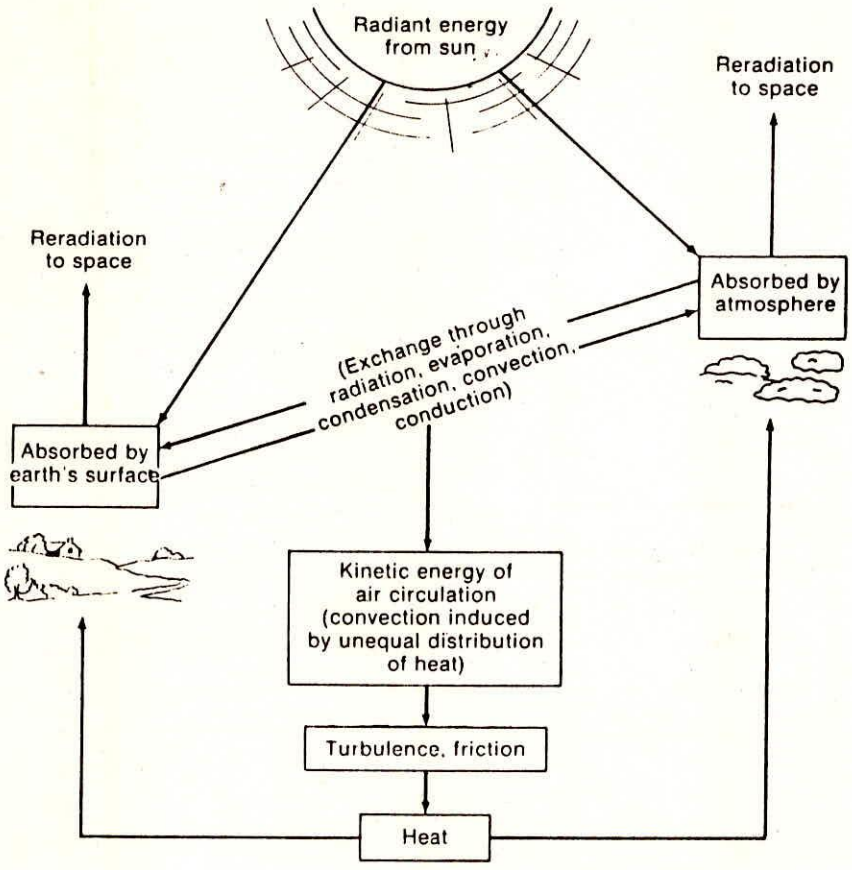

Fig. 2.1 Energy flow diagram

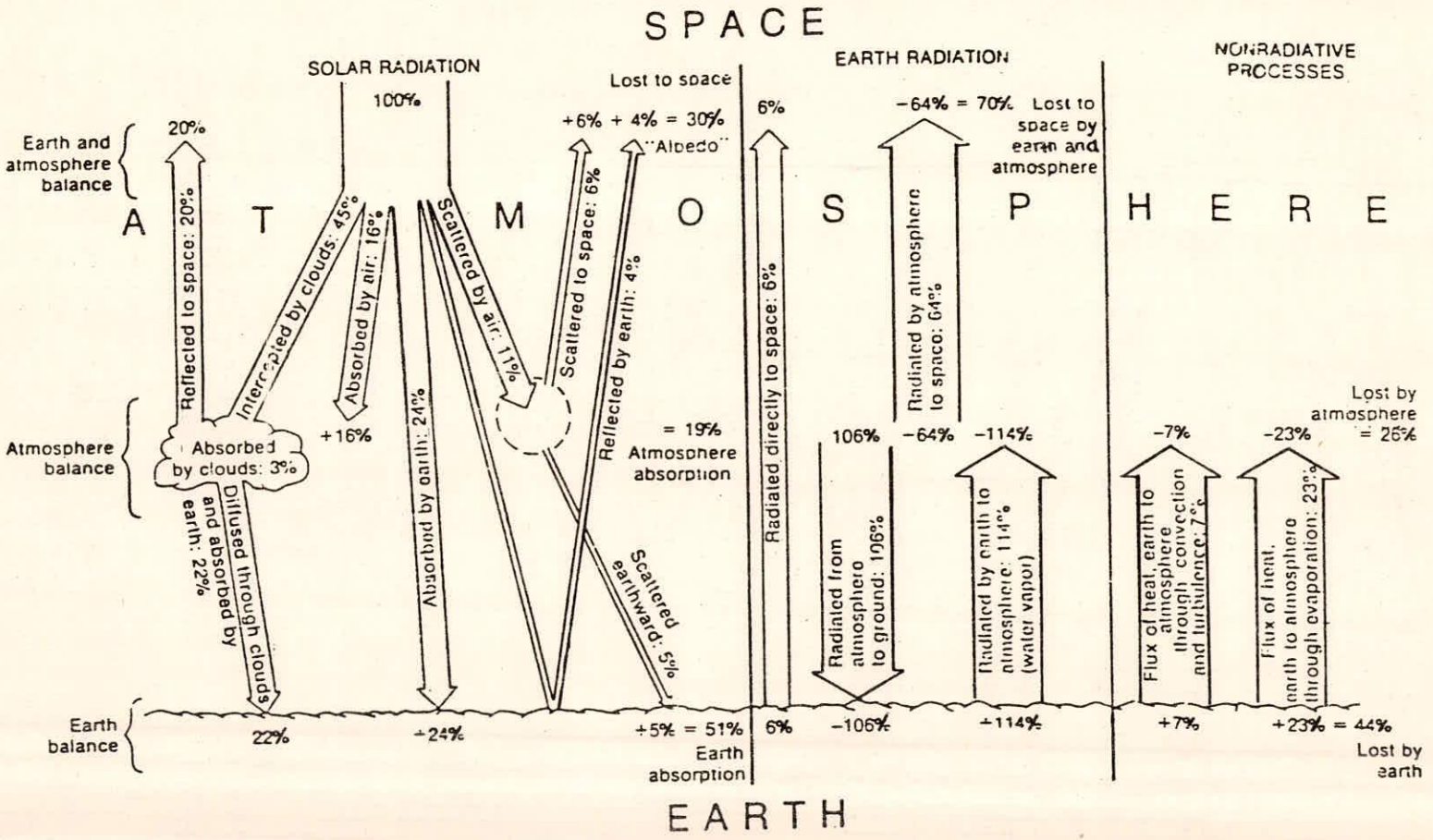

Fig. 2.2 Earth's energy budget

Table 2.1 Energy budget of the atmosphere ($cal/cm^2/min$)

I.	INCOME – Solar radiation		
	Average solar radiation received by earth and atmosphere:		0.50
	Absorbed by:		
	(a) atmosphere and clouds	0.10	
	(b) earth's surface	0.25	
	Net short-wave absorbed	0.35	
II.	OUTGO – Short-wave radiation		
	Lost to space by:		
	(a) reflection from clouds	0.10	
	(b) reflection from earth	0.02	
	(c) scattering from air	0.03	
	(i) Net short-wave outgo	0.15	
III.	OUTGO		
	The atmosphere:		
	(a) radiates to the earth	0.53	
	(b) radiates to space	0.32	
	(c) receives from earth through radiation	−0.57†	
	(d) receives from earth through convection, turbulence, and evaporation	−0.15	
	(ii) Net outgo from atmosphere	0.13	
	The earth:		
	(a) radiates to space	0.03	
	(b) radiates to the atmosphere	0.57	
	(c) loses to the atmosphere through convection and turbulence	0.04	
	(d) loses to the atmosphere through evaporation	0.11	
	(e) receives from the atmosphere through radiation	−0.53	
	(iii) Net outgo from earth	0.22	
IV.	TOTAL NET OUTGO (i + ii + iii)		0.50

for the planet as a whole, all parts of the earth and its atmosphere are not in radiative balance. In fact, it is the imbalance between the heat surplus received at the equator and the deficit at the poles that drives the atmospheric heat engine. The transfer of heat energy between these warm and cold regions of the earth produces the global wind system. The winds, in turn, reflect the work done by the atmospheric engine.

Of special interest on the long wave side (Fig.2.2 and III in table 2.1) is the fact that the amounts of radiative energy emitted by the air to the earth (106 percent or 0.53 cal/cm^2/min) and by the earth to the air (114 percent or 0.57 cal/cm^2/min) actually exceed the total solar energy absorbed by the earth. This is due to the blanketing effect of the atmosphere which keeps the earth's surface and lower layers of the atmosphere a good deal warmer than they would be without the atmosphere.

If the radiation budget at the earth's surface is expressed mathematically, the net radiation of a surface (R_n) is given as the algebraic sum of four radiative fluxes; the downward flux R_{sd} of solar radiation from sun and sky, the upward flux R_{su} of reflected solar radiation, the downward infrared or thermal radiation flux R_{id} from the atmosphere and the upward infrared radiation flux R_{iu} from the surface. Thus

$$R_n = R_{sd} - R_{su} + R_{id} - R_{iu} \qquad (2.1a)$$

The downward fluxes of solar and infrared radiation are controlled by atmospheric conditions. The upward solar radiation is that amount of the downward solar component that is reflected by the surface.

$$R_{su} = a\, R_{sd} \qquad (2.1b)$$

where a is the albedo or reflectivity. The upward infrared component is given by

$$R_{iu} = \varepsilon\, \sigma\, T_o^4 + (1 - \varepsilon)\, R_{id} \qquad (2.1c)$$

where, ε is the longwave emissisvity, σ the Boltzman constant and T_o the surface temperature.

Thus

$$R_n = (1 - a) R_{sd} + \varepsilon R_{id} - \varepsilon \sigma T_o^4 \qquad (2.1d)$$

2.1 Radiatively Important Atmospheric Constituents

The resulting changes in climate depend on the radiative properties of all radiative active atmospheric constituents. Table 2.2 lists the various atmospheric constituents and their volume mixing ratios (the number of molecules of the constituent in a unit volume divided by the number of molecules of air in that volume). Many constituents have volume mixing ratios that vary slowly in space and time. The constituents carbon dioxide (CO_2), methane (CH_4) and nitrous oxide (N_2O) are examples of species in this category. The CH_4 and N_2O mixing ratios are nearly constant with altitude through the troposphere, declining in the upper stratosphere as photolysis becomes more effective at high altitude. Other species are highly variable in both space and time. In addition to the species listed in Table 2.2, clouds and aerosols also are important radiatively active atmospheric constituents.

The atmospheric constituents differ greatly in their absorptive properties. The general characteristics of atmospheric absorption are shown in Fig. 2.3. The two curves in Fig. 2.3a show the energy distribution characteristics of black body emission at 6000 K (the solar temperature) and at 255 K (the average terrestrial emission temperature). The fractional absorption between the top of the atmosphere and ground level also is indicated as a function of wavelength in Fig. 2.3b .

There is very little gaseous absorption in the visible region (0.4-0.7 μm), although weak absorption bands of ozone and NO_2 occur in this region. Ozone is the primary absorber of solar radiation at ultraviolet (UV) wavelengths between 0.20 and 0.36 μm. In the solar near-infrared (IR) region (0.7-4 μm), water vapour (H_2O) is the most important absorber. Carbon dioxide has several absorption bands between 1.4 and 5.2 μm, with the two strongest bands centered at 2.7 and 4.3 μm.

The main gases of the atmosphere, nitrogen and oxygen, contribute only slightly to solar absorption. There are three weak oxygen absorption bands in the visible solar spectrum,

Table 2.2 : Atmospheric constituents and their volume mixing ratios

Constituent	Percent by Volume
Nitrogen (N_2)	78.084
Oxygen (O_2)	20.984
Argon (Ar)	0.934
Carbon Dioxide (CO_2)	0.033
Neon (Ne)	18.18×10^{-4}
Helium (He)	5.24×10^{-4}
Krypton (Kr)	1.14×10^{-4}
Hydrogen (H_2)	0.5×10^{-4}
Xenon (Xe)	0.089×10^{-4}
Methane (CH_4) (at surface)	1.7×10^{-4}
Nitrous Oxide (N_2O) (at surface)	0.3×10^{-4}

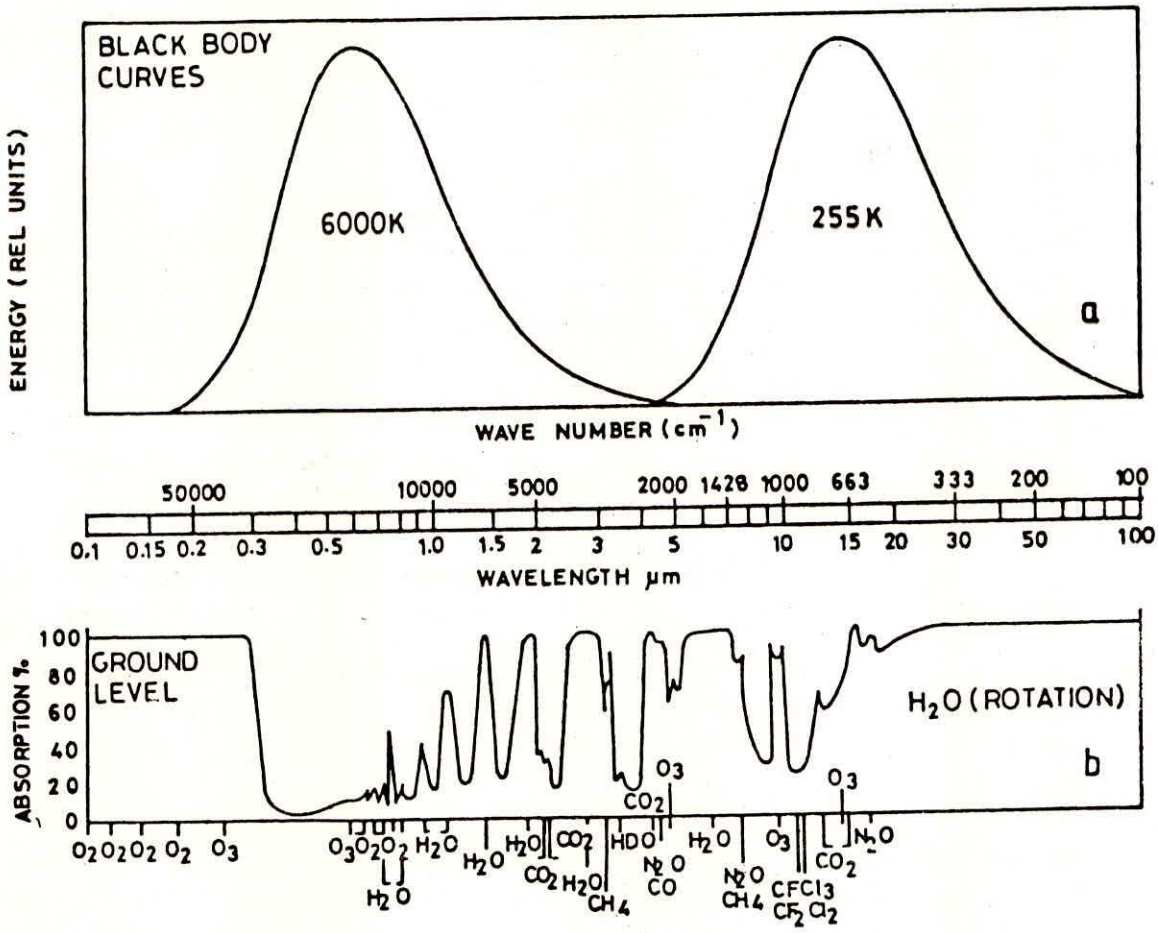

Fig. 2.3a Spectral distribution of the radiations from the sun and the earth corresponding to temp. of 6000 and 255 K

Fig. 2.3b Atmospheric absorption of the solar radiation by greenhouse gases

centered at wavelengths of 0.63, 0.69 and 0.76 μm respectively. Oxygen also has several systems of absorption bands in the far IR where there is little solar energy.

Many gases have absorption bands in the long wave region (wavelength >4 μm). Among these CO_2, H_2O and O_3, are the most important absorbers. CO_2 has strong absorption bands in the 15-μm region. The 15-μm band coincides with the peak in the thermal emission from the earth's surface. CO_2 absorbs upward radiation from below and replaces it with radiation emitted at the atmospheric temperature.

Water vapour absorption bands span most of the long wave region. Ozone has two narrow vibrational bands centered near 9.6 μm and a weak vibrational band centered at 14.27 μm that overlaps the strong 15-μm absorption band of CO_2. A strong absorption band at 4.7 μm is in a portion of the black body emission curve where there is little energy, so it does not contribute significantly to the long wave energy budget.

There is relatively little atmospheric absorption in the region between 800 and 1200 cm^{-1} except for continuum H_2O absorption in the lower tropical troposphere. Because the atmosphere is essentially transparent in this portion of the long wave regime, this region (centered at 10 μm) is called the atmospheric window.

Other radiatively active trace gases are listed in Table 2.3. Many of these gases have absorption bands that lie within the atmospheric window. Although the radiative effects of trace gases are currently small they could increase significantly in the future because the concentrations of many of the gases are projected to increase because of anthropogenic emissions.

2.2 Role of Greenhouse Gases in Affecting the Radiation Balance

Two gases- water vapour and carbon dioxide play the most important role in keeping the earth warm. Except for the atmospheric window, these gases block the direct escape of the infrared energy emitted by the earth's surface. Although the atmosphere absorbs only a small percentage of the shortwave solar radiation, it is quite opaque to the long-wave terrestrial

Table 2.3: Volume mixing ratios of trace gases other than CO_2

Trace Gas	Mixing Ratio in Lower Troposphere (ppm)
N_2O	0.3
CH_4	1.7
O_3	0.02-0.1
$CFCl_3$(CFC-11)	2.0×10^{-4}
CF_2Cl_2(CFC-12)	3.5×10^{-4}
CF_4	6.0×10^{-5}
CF_2HCI(CFC-22)	6.0×10^{-5}
CCl_4	1.5×10^{-4}
$CHCl_3$	1.0×10^{-5}
CH_2Cl_2	4.0×10^{-5}
CH_3Cl	6.5×10^{-4}
CH_3CCl_3	1.3×10^{-4}
C_2H_4	$1.0\text{-}20.0 \times 10^{-4}$
SO_2	1.0×10^{-4}
NH_3	1.0×10^{-3}
HNO_3	$1.0\text{-}10.0 \times 10^{-4}$

*ppm-Parts per million by volume

radiation. The heat retaining behavior of the atmosphere is somewhat analogous to what happens in a green house, and thus, the role of moisture and CO_2 in the atmosphere, allowing solar energy to pass through while absorbing much of the earth's long wave radiation, has thus come to be known as the GREENHOUSE EFFECT.

Trace gases that are radiatively active predominantly in the long wave region, such as CH_4, N_2O, $CFCl_3$ and CF_2Cl_2 have behaviours similar to that of CO_2. These gases are essentially transparent to solar radiation but are opaque to long wave radiation in specific spectral bands and they behave similarly to CO_2 in that they initially reduce the outgoing long wave radiation to space, which leads to a warming of the surface and troposphere until the radiation balance is restored.

Trace gases that are radiatively active in both the solar and long wave regions, such as O_3 and NO_2, can lead to either warming or cooling at the surface depending on how they are distributed vertically and on the relative strengths of the bands in the solar and long wave spectral regions.

Water vapour, CO_2 and O_3 are the most important radiatively active gases in terms of their contribution to the temperature structure of the atmosphere. The temperature structure of the atmosphere is shown in Fig. 2.4 . Fig. 2.5 shows the contribution of each of these gases to the net radiative heating rate as a function of altitude as computed by Manabe and Strickler (1964). This figure applies to global annual mean conditions. LH_2O, LCO_2 and LO_2 refer to individual contributions to the rate of temperature change that is due to long wave radiation absorption and emission. The curve marked $SH_2O+SCO_2+SO_3$ gives the rate of temperature change due to absorption of solar radiation by H_2O, CO_2 and O_3. Solar absorption by O_3 accounts for nearly all the solar absorption in the stratosphere (the region above 13 km), and H_2O is the major source of solar absorption by gases in the troposphere (<13 km). CO_2 is a very weak absorber of solar radiation, but it is very important in terms of the long wave cooling rates particularly in the stratosphere.

In the stratosphere, temperature increases with altitude

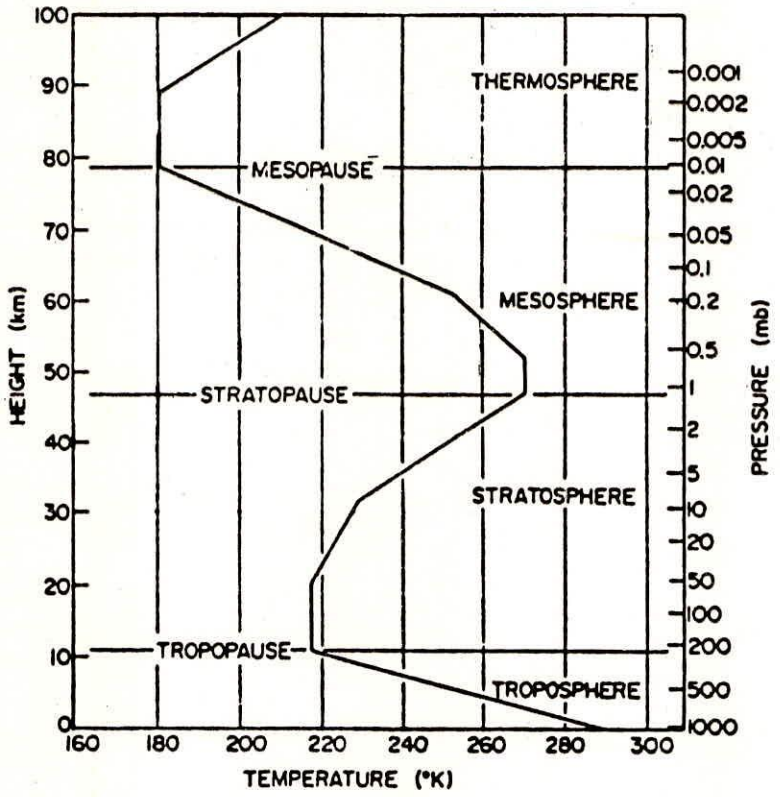

Fig. 2.4 Temperature structure of the atmosphere

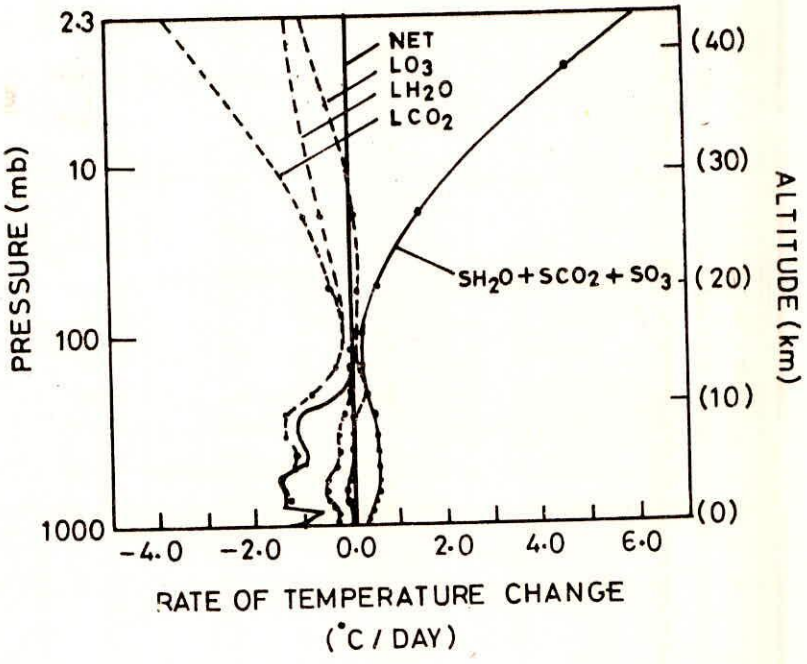

Fig. 2.5 Contribution of greenhouse gases to net radiative heating rates as a function of altitude, the letters L and S denote longwave and solar (Manabe and Strickler, 1964)

reflecting the heating due to absorption of solar radiation by O_3. On an annual average basis, the solar heating is compensated primarily by long wave cooling due to CO_2. The temperature profile in the troposphere ,with temperature decreasing with altitude, is a result of interactions between convection, large scale dynamics and radiation. Radiative processes in the troposphere contribute to the net energy balance of the troposphere surface system. The troposphere must radiate to space not only the solar energy absorbed there, but also the bulk of that absorbed at the surface.

Luther and Ellingson (1985) calculated the annual mean radiative budgets for stratosphere the troposphere and earth's surface respectively (Figs. 2.6 - 2.8). Because solar and long wave absorption almost exactly balance long wave emission, the stratosphere is very nearly in radiatively equilibrium. About 94% of that solar absorption in the stratosphere is contributed by O_3, with H_2O and CO_2 contributing the remaining 6%. The long wave absorption is more than twice the total solar absorption. The troposphere is highly opaque to long wave radiation, so only about 3% of the down ward emission reaches the earth's surface. Most of the absorbed long wave radiation in the stratosphere comes from troposphere emission rather than from the earth's surface.

Fig. 2.7 shows the radiative budget for the troposphere. Solar absorption in the troposphere equals about 18% of the solar radiation incident at the top of the atmosphere (342 w/m^2). Long wave absorption (primarily resulting from emission from the surface) amounts to more than 100% of the solar flux incident at the top of the atmosphere. The net excess of absorption over emission of 109 Wm^{-1} is balanced by the convective flux of latent heat and sensible heat from the earth's surface to the troposphere.

Long wave absorption is approximately twice the solar absorption for radiative budget for the earth's surface (Fig.2.8). Long wave emission from the surface is approximately 118 % of the incoming solar flux at the top of the atmosphere. The net long wave exchange between the surface and the atmosphere is a cooling of about 53 Wm^{-2}. The solar absorption is significantly greater than the net long wave emission, with the excess energy being transported to the troposphere as sensible and latent heat. Fig. 2.9 shows the global annual mean solar and long wave flux components. Since the convective mixing leads to strong coupling

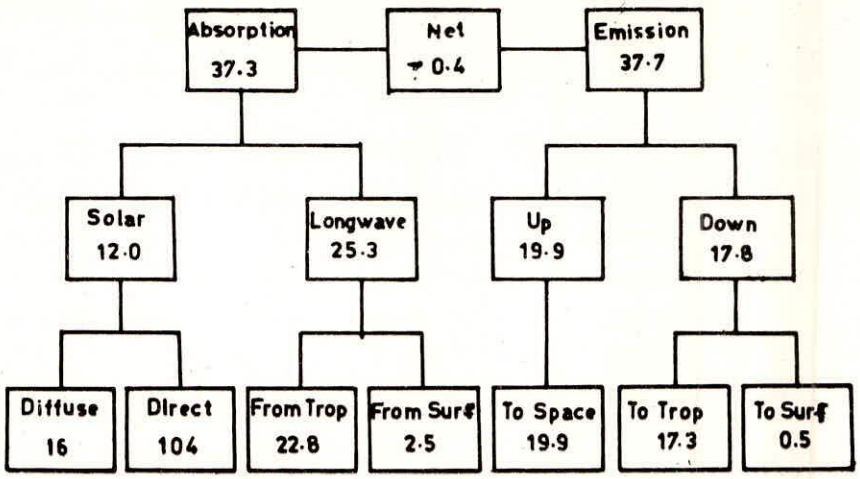

Fig. 2.6 Annual mean radiative budget for the stratosphere, energy components have units of W/m^2, (Luther and Ellingson,1985)

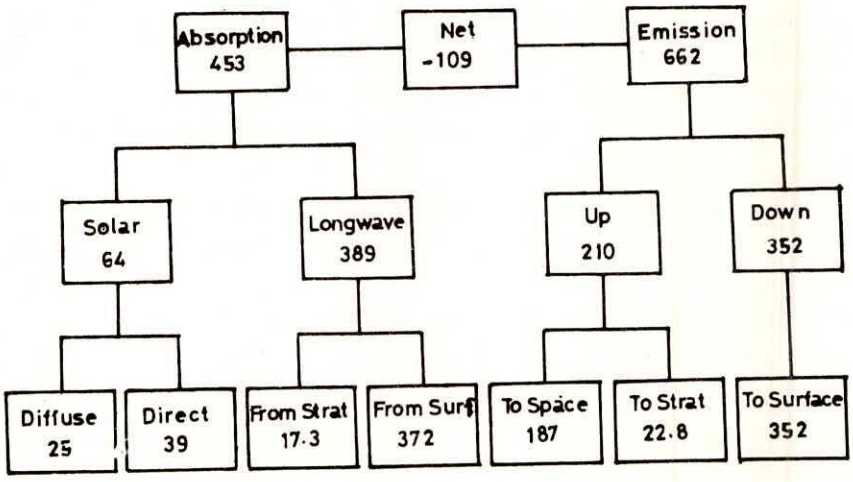

Fig. 2.7 Annual mean radiative budget for the troposphere, energy components have units of W/m^2, (Luther and Ellingson,1985)

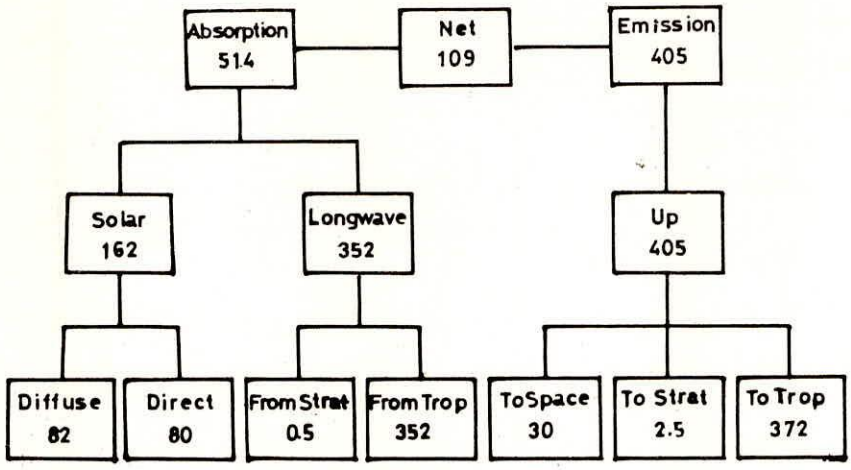

Fig. 2.8 Annual mean radiative budget for the earth's surface, energy components have units of W/m^2, (Luther and Ellingson, 1985)

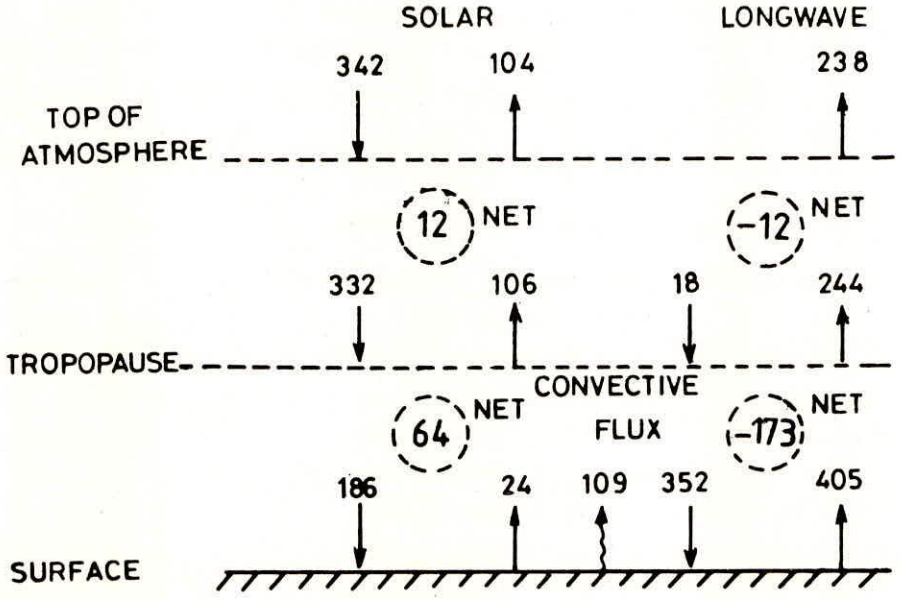

Fig. 2.9 Global annual mean solar and long wave flux components, energy components have units of W/m^2, (Luther and Ellingson, 1985)

between the upper and lower troposphere and also between the troposphere and earth's surface, the temperatures throughout the troposphere and at the surface are affected by changes in the net flux at the tropopause. Thus, a frequent basis for estimating the climate change resulting from a perturbation to the atmospheric composition is the effect the perturbation has on the net flux at the tropopause.

2.3 Trends of Increase in Greenhouse Gases

The concentrations of greenhouse gases viz. CO_2, CH_4, CFCs and N_2O in the atmosphere have increased since pre-industrial times due to human activities. The present and pre-industrial concentrations, current rates of change, present atmospheric lifetimes and sources of these gases are presented in Table 2.4 . Two other important greenhouse gases water vapour and ozone are not included in the table. The concentration of water vapour in the troposphere is determined internally within the climate system and on global scale, is not affected by human sources or sinks. Water vapour will increase in response to global warming and further enhance it, the process is included in climate models. The concentration of ozone is changing both in the stratosphere and troposphere due to human activities but it is difficult to quantify the changes from present observations.

Fig. 2.10 shows the changes in concentrations of CO_2, CH_4, N_2O and CFC from pre-industrial level. With increase in world's population resulting in more industrialization and agricultural developments the abundances of greenhouse gases have increased markedly. As can be seen in the figure the concentrations of carbon dioxide and methane have risen sharply after 18th century. The concentrations of nitrous oxide have increased since the mid 18th century, especially in the last few decades. CFCs were not present in the atmosphere before the 1930s.

3.0 ALBEDO - RADIATION CHARACTERISTICS OF UNDERLYING SURFACES

The determination of the radiation characteristics of the underlying surface is exceptionally important in taking account of the radiative interaction between the atmosphere and the underlying surface (see eq. 2.1). This refers above all to the albedo of the underlying surface, in other words the proportion of solar radiation reflected (or absorbed) by the surface. The range

Table 2.4: Summary of key greenhouse gases affected by human activities (IPCC ,1990)

	Carbon	Methane	CFC-11	CFC-12	Nitrous Oxide
Atmospheric concentration	ppmv	ppmv	pptv	pptv	ppbv
Pre-industrial (1750-1800)	280	0.8	0	0	288
Present day (1990)	353	1.72	280	484	310
Current rate of change per year	1.8 (0.5%)	0.015 (0.9%)	9.5 (4%)	17 (4%)	0.8 (0.25%)
Atmospheric life-time (years)	(50-200)+	10	65	130	150

ppmv = parts per million by volume;

ppbv = parts per billion (thousand million) by volume;

pptv = parts per trillion (million million) by volume.

+ the way in which CO_2 is absorbed by the oceans and biosphere is not simple and a single value cannot be given

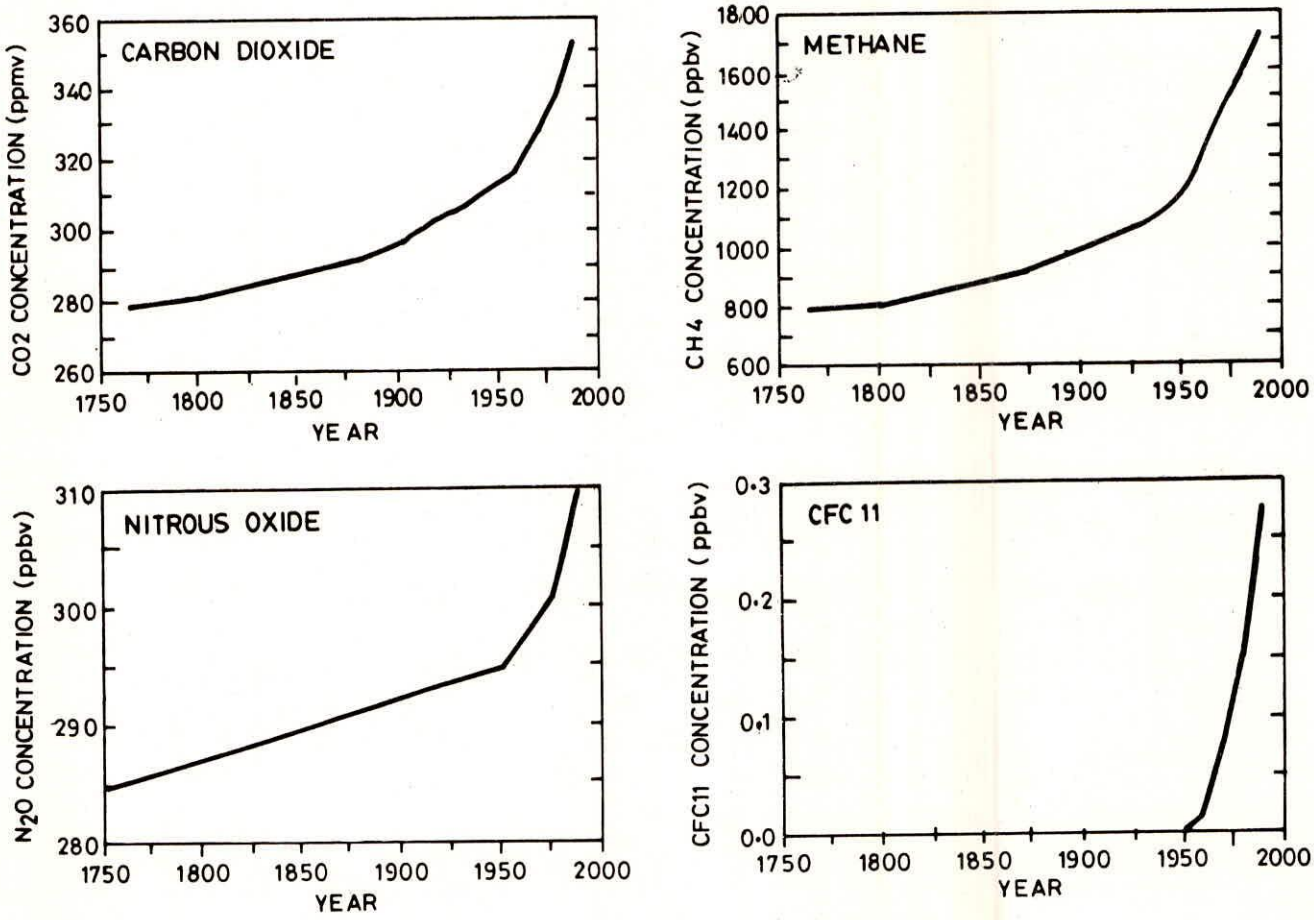

Fig. 2.10 Concentrations of carbon dioxide, methane, nitrous oxide and chlorofluoro carbons (IPCC,1990)

of published albedo values for characteristic surface types has been compiled by Kukla and Robinson (1980) and is given in Table 3.1.

This is large in most of the categories because the albedo varies not only with respect to material composition, but also with roughness, moisture content, solar angle, angular and spectral distribution of ground level irradiation etc. Most surfaces when moist have an albedo several percent lower than when dry. Outside the snow and ice boundaries the variation in surface moisture accounts for a large part of intra-annual albedo variability. The angular and spectral distribution of incoming radiation significantly influences surface albedo in the high and middle latitudes during cold season when the atmospheric humidity is low. It plays a minor role, if any, in temperate latitudes. Kukla and Robinson (1980) presented the monthly and annual average surface albedo estimates for different latitudes (Table 3.2). The latitudinal distribution of annual average zonal surface albedo is shown in Fig. 3.1.

The albedo of natural surface is an essential input parameter for climate models. Sensitivity studies have shown that the climate is sensitive to surface albedo changes. Thus, alteration in the albedo due to increase in greenhouse gas concentration could affect the climate considerably. Original studies by Charney (1975) involved the use of a simple theoretical model of the directly driven circulation caused by a change in the heating pattern induced by a surface albedo change. Because this study required many assumptions, Charney et al (1977) performed a more realistic experiment with the NASA Goddard Institute for Space Studies (GISS) GCM. In this experiment the albedo over desert regions was increased from 0.14 to 0.35. Separate experiments were carried out assuming fixed ground wetness and surface hydrology. The precipitation with each type of surface witness decreased over the deserts, resulting in an increase of surface albedo. The surface albedo increased to the south of the deserts.

Similar experiments were performed with the two dimensional zonal average atmospheric model by Eilsaesser et al (1976). They found that increased albedo in the region led to pronounced decrease of precipitation over and around deserts and increases in precipitation to the south of desert. Chervin (1979) conducted similar experiments with the NCAR third generation GCM in which the surface albedo over the modeled United States and Sahara desert regions was increased from 0.07 to 0.17 for the

Table 3.1: Range of published surface albedo values for different surface types

Surface type	Range
Snow-free and ice-free surfaces	
1. Water bodies between 90°-60°	6-44%
2. Water bodies between 0-60°	5-20%
3. Tropical rainforest	7-15%
4. Naturally vegetated terrain, farmland, common soils, stony deserts, etc.	7-25%
5. Semi-deserts and deserts with light colored soils	20-33%
6. Deserts with light colored sands, salt playas, etc.	28-44%
Snow-covered land	
1. Mountains with scattered snow	
2. NOAA reflectivity Class 1	25-35%
3. NOAA reflectivity Class 2	35-55%
4. NOAA reflectivity Class 3	60-70%
5. Snow-covered ice sheets and ice caps in the Arctic and Antarctica	75-89%

Table 3.2: Summary of latitudinal distribution of average surface albedo estimates (%) (Kukla and Robinson, 1980)

	Month												
	Jan.	Feb.	Mar.	Apr.	May	June	July	Aug.	Sep.	Oct.	Nov.	Dec.	Annual mean
Northern Hemisphere													
60-90°N	61.6	61.2	61.0	58.1	55.5	45.1	32.2	28.1	32.0	44.4	53.7	61.5	49.5
30-60°N	22.7	24.6	22.5	17.8	15.6	13.7	12.8	12.7	12.9	14.6	16.4	21.2	17.3
0-30°N	10.9	10.3	10.3	10.3	10.2	10.2	10.2	10.2	10.2	10.3	10.5	10.8	10.4
0-90°N	22.1	22.4	21.6	19.5	18.3	16.2	14.1	13.5	14.1	16.5	18.5	21.5	18.2
0-90° (land)	33.8	35.4	34.0	29.4	27.4	23.2	20.9	20.4	20.8	25.1	27.6	32.6	27.6
0-90° (Ocean)	14.4	13.9	13.5	13.0	12.4	11.6	9.7	9.0	9.7	10.8	12.5	14.2	12.1
Southern Hemisphere													
60-90°S	46.5	44.0	46.1	53.1	61.6	67.7	72.8	74.4	74.5	73.5	67.1	56.1	61.5
30-60°S	7.2	7.2	7.7	8.7	9.8	10.6	10.9	9.9	10.3	9.7	8.2	7.5	9.0
0-30°S	8.2	8.2	8.2	8.3	8.9	9.1	8.6	8.5	8.3	8.2	8.2	8.2	8.4
0-90°S	13.0	12.6	13.1	14.5	16.3	17.6	18.1	18.0	18.0	17.5	16.1	14.4	15.8
0-90°S (land without Antarctica)	16.3	16.2	16.2	16.2	16.3	17.0	17.0	17.0	16.7	16.5	16.4	16.4	16.5
0-90°S (Ocean with Antarctica)	12.5	12.1	12.6	14.2	16.3	17.6	18.3	18.2	18.2	17.7	16.1	14.1	15.7
Globe													
90°S-90°N	17.5	17.5	17.4	17.0	17.3	16.9	16.1	15.7	16.0	17.0	17.3	17.9	17.0
90°S-90°N (land without Antarctica)	29.4	30.6	29.5	26.1	24.6	21.6	19.9	19.5	19.8	22.9	24.8	28.5	24.8
90°S-90°N (Ocean with Antarctica)	13.3	12.8	13.0	13.7	14.7	15.1	14.8	14.4	14.7	14.9	14.6	14.1	14.2

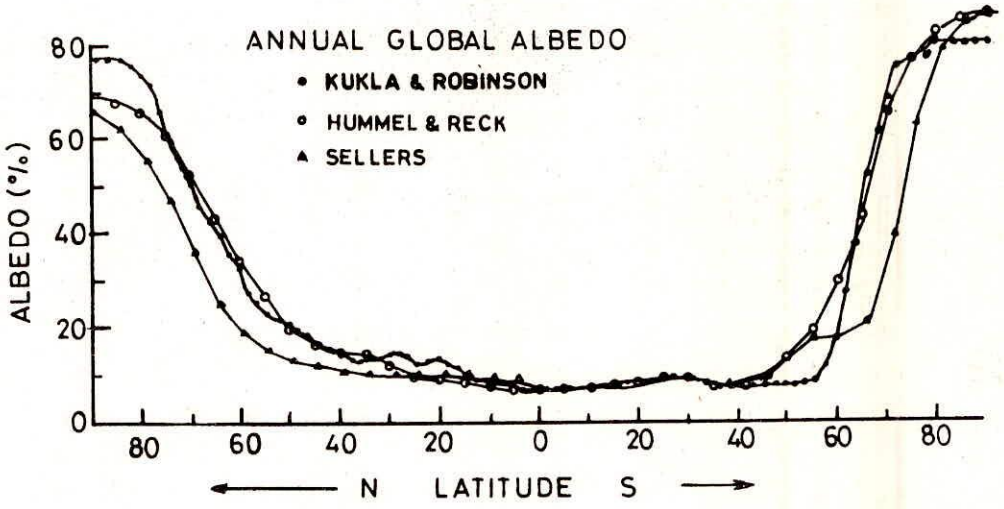

Fig. 3.1 Latitudinal distribution of annual average zonal surface albedo, (Kukla and Robinson, 1980)

former region and from 0.08 to 0.45 for the latter. Chervin also found changes in the pattern of precipitation similar to those of earlier studies. In summary, the results support the general hypothesis that biogeophysical processes involving increased surface albedo can lead to further drying, which in turn can lead to even higher surface albedo and considerable change in climate.

4.0 EVAPORATION

Evaporation and transpiration form important links in the hydrological cycle in which water is transferred to the atmosphere as water vapour. There are three prerequisites for evapotranspiration to occur. These are a source of water, energy to drive the phase change and a sink for water or the moisture deficit in the air above the ground. Changes in any of these would result in considerable changes in evapotranspiration. Changes in net solar radiation due to increase in greenhouse gases which generally drives the phase changes may affect the evapotranspiration from the surface.

Studies have been carried out on effect of climate change on evapotranspiration using different methodical approaches. Some of them consider the changes as a function temperature (Revelle and Waggoner, 1983; Gleick, 1987), as a function of the CO_2 effects on plant resistance (Aston, 1984; Idso and Brazel, 1984) and using micrometeorological and physiological measurements (Martin et al, 1989). Besides these off - line studies global climate models have also been used to study the changes in latitudinal distribution of zonal mean evaporation rate under the increased greenhouse gases scenario (Manabe and Stouffer, 1980)

Aston (1984) used a distributed deterministic process model WATSIM (Aston and Dunin, 1980) to simulate the effects of changed stomatal resistance (the stomatal resistance rises with CO_2 increase) on streamflow of a 5 ha experimental catchment. The evaporation was computed using

$$EP = [S/(S+\gamma)](R-G) + (\rho\ Cp/ra)\ (T-T_w) \qquad (4.1)$$

and

$$ET = EP/[1+\gamma/(s+\gamma)\ (r_c/r_a)] \qquad (4.2)$$

Where ; EP - potential evaporation,
ET - actual evaporation,
s - slope of the saturation vap. project curve

γ - psychrometric constt.
R - net radiation
G - ground heat flux
ρ - air density
C_p - heat capacity of air at constt. pressure
T & Tw - ambient dry & wet bulb temp.
r_a & r_c - aerodynamic and canopy resistances respectively

Figure 4.1 shows the results of simulation of the impact of CO_2 increase on catchment water yield in 1973. The months with small to intermediate yields were relatively more sensitive to CO_2 increase as the evaporation process was limited by the soil moisture.

Aston (1984) simulated a large catchment area (417 km^2) using a hydrological model SHOLSIM evolved from WATSIM. The major difference between the two was in the formulation of evapotranspiration. In SHOLSIM, ET was expressed as a ratio of class A pan evaporation and related to the absolute values of soil moisture content:

$$ET/Pan = S_p (\theta - \theta_w)$$

where, S_p is the empirically derived slope of the relationship between pan ratio and moisture content for a given vegetation type, θ and θ_w are the volumetric soil moisture content and moisture content at 15 atm. respectively and Pan is the evaporation from the class A pan evaporimeter. A doubling of resistances in eq. (4.2) resulted in a reduction of ET of around 20-40%, depending on ambient conditions. The present level of water yield of both small and large catchments can significantly increase due to doubling of CO_2 concentrations.

Bultot et al (1988) evaluated quantitatively the impact of the CO_2 doubling on the annual regime of the effective evapotranspiration and other energy balance components. They used IRMB conceptual daily step model to simulate the daily effective evapotranspiration for a drainage basin in Belgium. Besides daily effective evapotranspiration, the model quantitatively estimated the annual regimes of net terrestrial radiation and net radiation for the

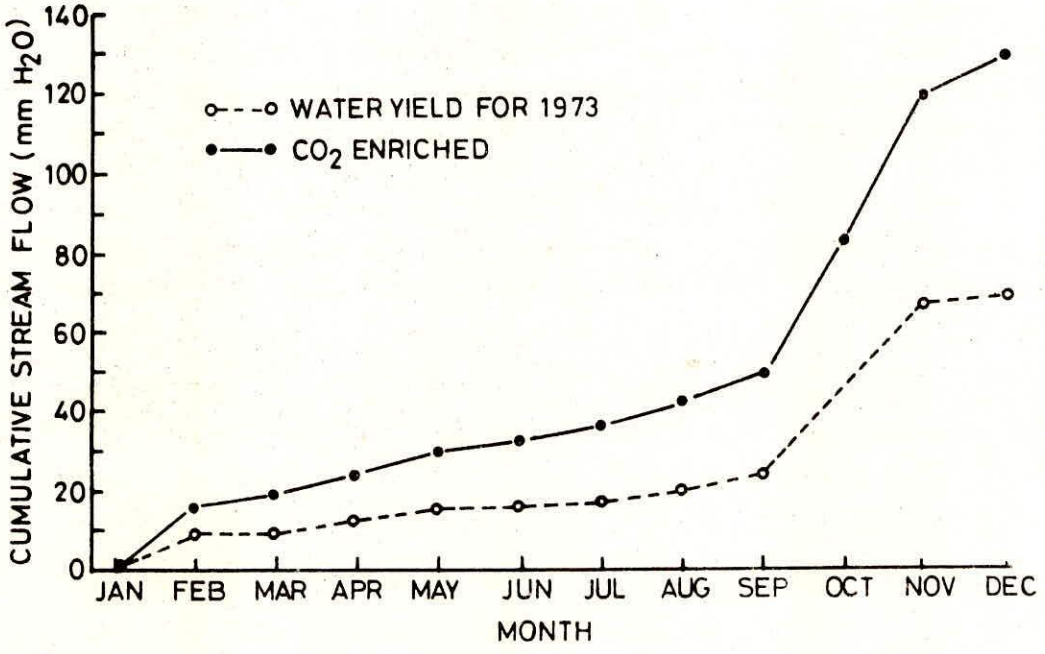

Fig. 4.1 Simulation of impact of CO_2 increase on catchment yield in 1973 (Aston ,1984)

$2 \times CO_2$ case and on the basis of a ten year period daily data for the Semois drainage basin.

The compared regimes of the evapotranspiration and of other climate and hydrological variables under the present climatic conditions (scenario 0) and assuming a doubling of the atmospheric CO_2 concentration (scenario 1), as studied by Bultot et al (1988) are given in Table 4.1 . The potential evapotranspiration increases in all seasons, as one goes from scenario 0 to scenario 1; the maximum and minimum being during April (0.3 mm d^{-1}) and January (0.06 mm d^{-1}) respectively. However, in relative values the rise is greatest during winter months the reason being the smallness of the corresponding present day ETP values. In response to the increased potential evapotranspiration, the effective evapotranspiration also augments, though not in the same ratio. This is because in scenario 1, the rainfall is lowered during the late spring and summer and the water supply from the soil cannot meet fully the evapotranspiration requirements.

Martin et al. (1988) studied the sensitivity of evapotranspiration in a wheat field, a forest and a grassland to changes in climate and direct effects of carbon dioxide using the equation

$$LE = \frac{s(R_n+S) + \rho_a C_p (e_s-e)/r_a}{s + \gamma \left(\frac{r_a+r_c}{r_a}\right)} \qquad (4.3)$$

where L is the latent heat of vaporization in J kg^{-1}, E the flux of evaporated water in kg $m^{-2} s^{-1}$, R_n the net radiation in W m^{-2}, S the soil heat flux in W m^{-2}, ρ_a the density of dry air in kg m^{-3}, r_a and r_c, the aerodynamic and canopy resistances in sm^{-1}, C_p the specific heat of dry air at constant pressure in J $kg^{-1} K^{-1}$, e_s the saturation partial pressure of water vapour at leaf temperature, e the actual vapour pressure in the air above the canopy, both in Pa, and, s and γ are the derivative of the saturation vapour pressure with respect to temperature and the pyschrometric constt. respectively, both in Pa K^{-1}.

Table 4.1 : Climatic and hydrological variables under scenario 0 and scenario 1 (Bultot et al, 1988)

	J	F	M	A	M	J	J	A	S	O	N	D	Year
Potential evapotranspiration (mm d^{-1})													
ETP_0	0.149	0.373	0.805	1.768	2.744	3.130	3.132	2.721	1.881	0.890	0.258	0.167	1.507
ETP_1	0.211	0.551	1.061	2.069	2.950	3.377	3.337	2.997	2.015	0.995	0.359	0.233	1.685
ΔETP	0.062	0.178	0.256	0.301	0.206	0.247	0.204	0.276	0.134	0.105	0.101	0.067	0.178
$\Delta ETP/ETP_0$	42%	48%	32%	17%	8%	8%	7%	10%	7%	12%	39%	40%	12%
Effective evapotranspiration (mm d^{-1})													
ET_0	0.149	0.370	0.793	1.690	2.608	2.778	2.766	2.266	1.611	0.834	0.255	0.167	1.362
ET_1	0.211	0.546	1.042	1.965	2.773	2.936	2.868	2.391	1.655	0.920	0.353	0.233	1.496
ΔET	0.062	0.176	0.249	0.275	0.165	0.158	0.102	0.125	0.044	0.086	0.098	0.066	0.134
$\Delta ET/ET_0$	42%	48%	31%	16%	6%	6%	4%	6%	3%	10%	38%	40%	10%
ET_0/ETP_0	100%	99%	99%	96%	95%	89%	88%	83%	86%	94%	99%	100%	90%
ET_1/ETP_1	100%	99%	98%	95%	94%	87%	86%	80%	82%	92%	98%	100%	89%
Water vapour pressure (hPa)													
e_0	5.96	5.98	6.58	7.46	10.14	12.62	14.09	13.98	11.89	9.55	7.46	6.38	9.36
e_1	7.42	7.60	8.32	9.21	12.19	15.00	16.51	16.18	13.82	11.44	9.05	7.99	11.25
Δe	1.46	1.62	1.74	1.75	2.05	2.38	2.42	2.20	1.93	1.89	1.59	1.61	1.89
$\Delta e/e_0$	24%	27%	26%	23%	20%	19%	17%	16%	16%	20%	21%	25%	20%
Temperature (°C)													
t_0	0.7	1.4	3.4	6.1	10.9	14.0	15.7	15.3	11.8	8.0	3.9	1.6	7.8
t_1	3.8	4.8	6.8	9.2	13.7	16.7	18.2	17.6	14.1	10.7	6.7	4.3	10.6
Δt	3.1	3.4	3.4	3.1	2.8	2.7	2.5	2.3	2.3	2.7	2.8	3.2	2.8
Precipitation (mm d^{-1})													
P_0	3.47	3.42	3.35	2.37	3.07	2.62	2.74	2.12	2.71	2.31	4.77	3.77	3.06
P_1	3.77	3.79	3.67	2.71	3.03	2.53	2.69	2.05	2.71	2.48	5.04	4.05	3.21
ΔP	0.30	0.37	0.32	0.34	−0.04	−0.09	−0.05	−0.07	0.00	0.17	0.27	0.28	0.15
$\Delta P/P_0$	9%	11%	10%	14%	−1%	−3%	−2%	−3%	0%	7%	6%	7%	5%
ET_0/P_0	4.3%	10.8%	23.7%	71.2%	84.9%	106.0%	100.9%	106.9%	59.4%	36.1%	5.3%	4.4%	44.6%
ET_1/P_1	5.6%	14.4%	28.4%	72.5%	91.5%	116.0%	106.6%	116.7%	61.1%	37.1%	7.0%	5.8%	46.7%
Water content of the upper layer of the unsaturated zone (percentage of values at saturation) – Maximum water capacity: WSX = 23 mm													
WS_0/WSX	100%	98%	91%	71%	66%	54%	54%	54%	59%	82%	98%	100%	77%
WS_1/WSX	100%	96%	88%	69%	63%	50%	51%	49%	56%	80%	97%	99%	75%
Water content of the lower layer of the unsaturated zone (mm and percentage of values at saturation)													
WIX	194.1	194.1	195.1	198.7	203.6	208.5	211.1	210.0	205.3	201.0	196.8	193.9	201.0
WI_0/WIX	100%	100%	100%	97%	91%	83%	78%	74%	72%	80%	93%	100%	89%
WI_1/WIX	100%	100%	99%	96%	89%	79%	73%	68%	65%	74%	90%	100%	86%

Table 42: Sensitivity of evapotranspiration to climate change and direct effects of CO_2 in a wheat field, a forest and a grassland (Martin et al. 1989)

Line no.	Change in T (K)	R_n (%)	e (%)	r_s (%)	LAI (%)	Wheat LE (W m^{-2})	Wheat Change (%)	Forest (avg. all days) LE (W m^{-2})	Forest Change (%)	Grassland LE (W m^{-2})	Grassland Change (%)	Notes
												Climate Change Scenario I
1	3	10	−10	0	0	562	33	350	40	302	29	1) Climate change only
2	3	10	−10	20	0	528	25	321	28	276	18	2) Climate change + stomatal resistance increase
3	3	10	−10	40	0	499	18	298	19	254	9	
4	3	10	−10	60	0	473	12	277	11	235	1	
5	3	10	−10	0	15	589	39	372	49	321	38	3) Climate change + leaf area index increase/ decrease
6	3	10	−10	0	−15	530	25	324	30	279	20	
7	3	10	−10	20	15	556	31	343	37	295	27	4) Climate change + change in stomatal resistance and leaf area index
8	3	10	−10	20	−15	496	17	297	19	253	9	
9	3	10	−10	40	15	527	24	319	27	273	17	
10	3	10	−10	40	−15	466	10	273	9	232	−1	
11	3	10	−10	60	15	501	18	298	19	254	9	
12	3	10	−10	60	−15	440	4	254	1	214	−8	
												Climate Change Scenario II
13	3	−10	10	0	0	455	7	272	9	246	6	1) Climate change only
14	3	−10	10	20	0	428	1	250	0	225	−3	2) Climate change + stomatal resistance increase
15	3	−10	10	40	0	404	−5	232	−7	207	−11	
16	3	−10	10	60	0	383	−10	216	−14	192	−18	
17	3	−10	10	0	15	477	13	290	16	262	12	3) Climate change + leaf area index increase/ decrease
18	3	−10	10	0	−15	429	1	253	1	227	−2	
19	3	−10	10	20	15	450	6	267	7	241	3	4) Climate change + change in stomatal resistance and leaf area index
20	3	−10	10	20	−15	401	−5	231	−8	206	−11	
21	3	−10	10	40	15	427	1	248	−1	223	−4	
22	3	−10	10	40	−15	377	−11	213	−15	189	−19	
23	3	−10	10	60	15	406	−4	232	−7	208	−11	
24	3	−10	10	60	−15	356	−16	197	−2	174	−2	

Martin et al (1988) calculated the LE flux using actual weather and plant parameter values as temperature, net radiation, air humidity, wind speed, leaf area index, characteristic leaf dimension and stomatal resistance. They tested the sensitivity of ET to each individual climate and plant factor, changing each factor at a time, two factors at a time and then changing them in groups ; the range of changes in climatic parameters was obtained from literature. Table 4.2 gives the simulated effects of climatic change on LE, when various parameters are changed simultaneously. These studies showed that when all the climatic and plant factors are considered evaporation estimates can differ greatly from those that consider only temperature.

5.0 INCREASE IN GREENHOUSE GASES AND CLIMATE MODEL IMPLICATIONS

5.1 Radiation and Albedo

There have been several recent model studies of the effect of increased CO_2 concentrations on the atmospheric radiation budget (Augustsson and Ramanathan, 1977; Ramanathan et al, 1979; Hansen et al, 1981; Ramanathan, 1981; Kiehl and Ramanathan, 1982; Wang and Ryan, 1983). All these model studies show that increased CO_2 would reduce the long wave radiative loss by the troposphere - surface system, which would result in an increase in temperature.

The direct radiative forcing due to a doubling of CO_2 is the change in radiative flux densities that would occur while holding all other parameters fixed (no change in atmospheric temperature, moisture content, etc.). The increase in downward longwave flux at the surface when CO_2 is doubled has been calculated to be 1.1 - 1.8 Wm^{-2} (Ramanathan et al, 1979; Hansen et al, 1981; Ramanathan, 1981). The magnitude varies with latitude, being smallest at low latitudes and largest at high latitudes. This latitude variation results from the variation in water vapour abundance.

The direct radiative heating of the surface troposphere system because of doubled CO_2 with no change in atmospheric temperatures or H_2O amounts is about 4 Wm^{-2} averaged

hemispherically, ranging from nearly 5 Wm^{-2} at low latitudes to about 2 Wm^{-2} at high latitudes. This forcing also has a little seasonal dependence (Ramanathan et al, 1979), with little seasonal variation at low latitudes and a range (maximum to minimum) of about 1 Wm^{-2} at high latitudes. The maximum heating occurs in summer and the minimum in winter.

In the stratosphere, increased CO_2 concentration results in enhanced longwave emission to space and an increase in downward emission to the troposphere. The downward emission to the troposphere increases by 1-2 Wm^{-2}, the smallest value occurring at low latitudes and the largest at high latitudes.

An increase in CO_2 concentration also affects solar absorption in the atmosphere. For doubling of CO_2 the increased solar absorption by CO_2 is about 0.4 Wm^{-2}. By absorbing more solar radiation, CO_2 allows less radiation to reach the earth's surface. The reduction in solar radiation absorbed by the earth's surface is about 0.3 Wm^{-2}, thus the net change for the atmosphere - surface system is an increase of only about 0.1 Wm^{-2} in solar absorption. Consequently increased CO_2 does not have a significant direct effect on net solar heating of the atmosphere but it does effect the partitioning between atmospheric and surface absorption (Luther and Ellingson, 1985).

Following the initial radiative forcing when CO_2 is doubled, there is an increase in downward flux to the surface as the atmosphere warms. The increased tropospheric temperatures lead to enhanced long wave emission by all of the radiatively active constituents, namely CO_2, H_2O, O_3, clouds and trace gases. As the surface and troposphere warm, increased evaporation leads to increase in absolute humidity which acts to reduce long wave emission from the surface to space (leading to further heating of the troposphere) and enhances long wave emission from the atmosphere to the surface.

Chou et al (1982) , using the GLAS multi layer energy balance model studied the climatic response to CO_2 changes, where the forcing is essentially radiative. Fig. 5.1 shows the latitudinal distribution (zonally and annually averaged) of change in the surface heat budget due to change in CO_2. With doubling

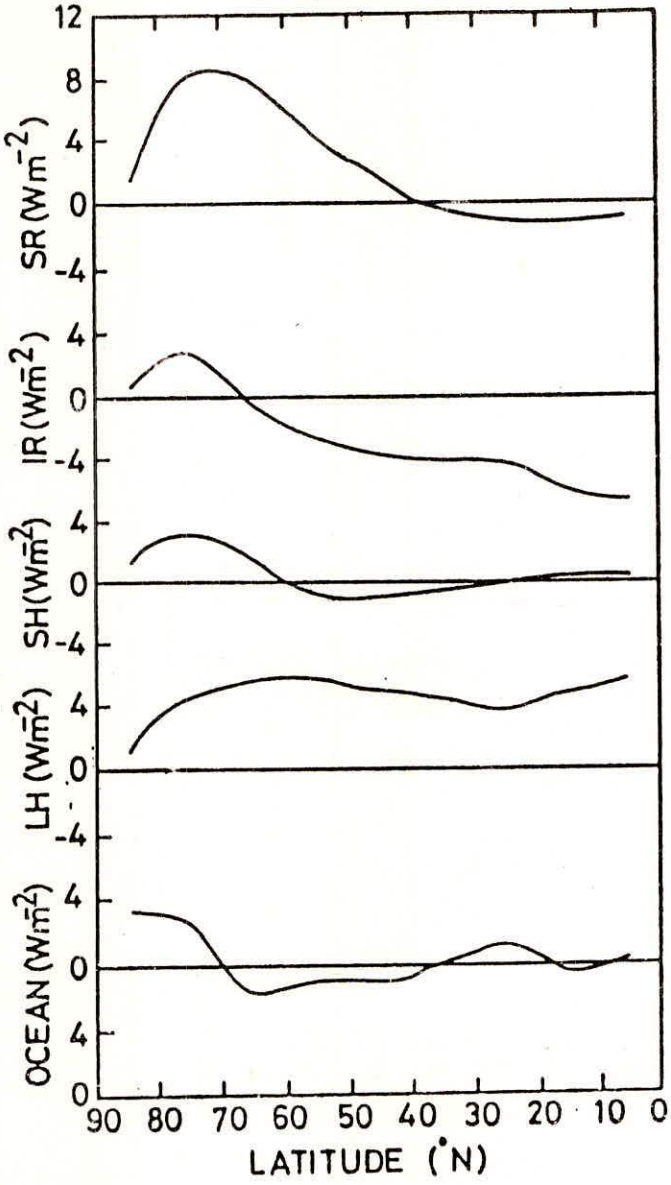

Fig. 5.1 Latitudinal distribution of the changes in surface heat flux due to a doubling of the CO_2 content (Chou et al , 1982)

SR - Absorption of solar radiation
IR - Net upward infrared radiation
SH - Sensible heat flux
LH - Latent heat flux
Ocean - Heating due to ocean transport

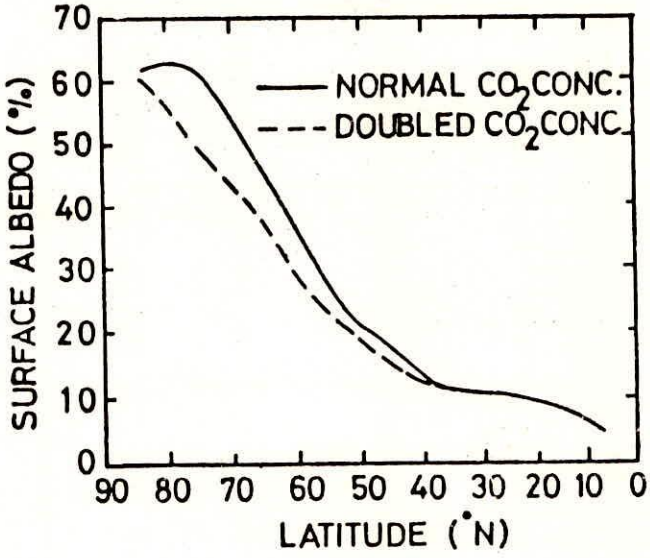

Fig. 5.2 Latitudinal distribution of the surface albedo for normal and doubled CO_2 concentrations, (Chou et al, 1982)

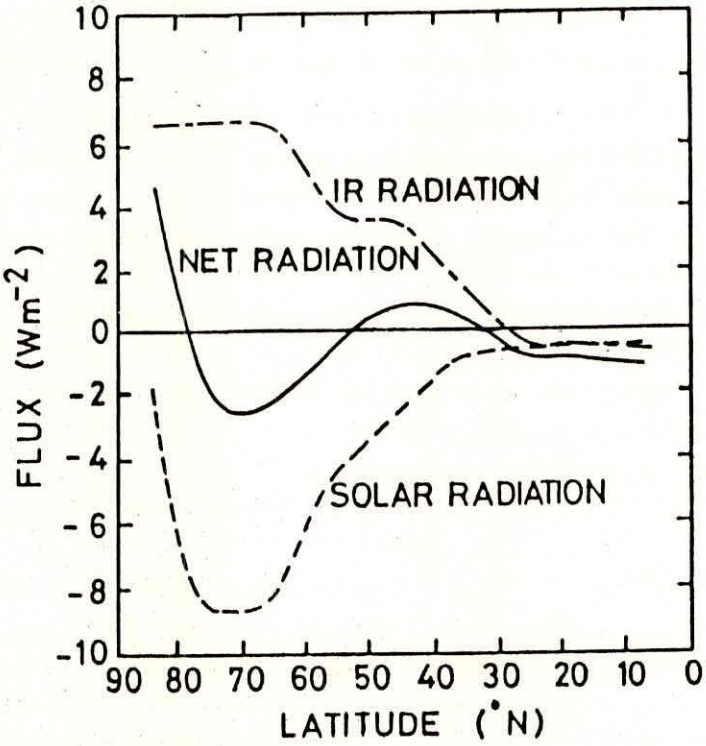

Fig. 5.3 Changes in upward radiation fluxes at the top of the atmosphere for doubling of CO_2 content, (Chou et al, 1982)

CO_2 solar radiation absorbed at the surface in tropics decreases slightly due to a more humid atmosphere which reduces the amount of solar radiation incident at the surface. The absorption of solar radiation increases pole ward of 40° N and reaches a maximum at 75°, that is consistent with the increase in surface albedo (Fig.5.2).

Chou et al (1982) found that except in the polar region where the increase in the surface temperature is the largest, the increase in the downward IR flux exceeds that in the upward flux due to the increase in water vapour content. The result is a reduced net upward IR flux for a doubled CO_2 content.

The changes arising from a doubled CO_2 in solar and IR radiation at the top of the atmosphere are shown in Fig. 5.3. The absorption of solar radiation increases at all latitudes. It can be seen from Fig. 5.1 and 5.3 that the increase in absorption of solar radiation at low latitudes is in the atmosphere due to higher water vapour content and the increase at high latitudes is mostly at the surface due to smaller ice/ snow cover. In the infrared, the change also increases from low to high latitudes. At low latitudes the negative change is dominated by the negative temperature change in the stratosphere. At high latitudes the large positive change is due to a large increase in the surface temperature accompanied with a relatively transparent atmosphere.

Manabe and Stouffer (1980) used a general circulation model of the atmosphere with a limited computational domain, idealized geography and annual mean insolation. They studied the sensitivity of the radiation budget to quadrupling of atmospheric CO_2. They first reproduced the overall radiation budget of the joint atmosphere ocean continent system. Fig. 5.4 illustrates the seasonal variation of hemispheric and global mean values of solar, terrestrial and net radiative fluxes at the top of model atmosphere. They evaluated the latitudinal distribution of difference in the net incoming solar radiation between the $4xCO_2$ and $2xCO_2$ experiment at the top of model atmosphere (Fig. 5.5). They found that the difference in the northern hemisphere increases with increasing latitude pole wards of 30°N, whereas in the southern hemisphere, the difference has local maximum along the periphery of the Antarctic continent, but it is smaller over the continent. The northern hemisphere change of the net incoming solar radiation (or planetary albedo), which is caused by the

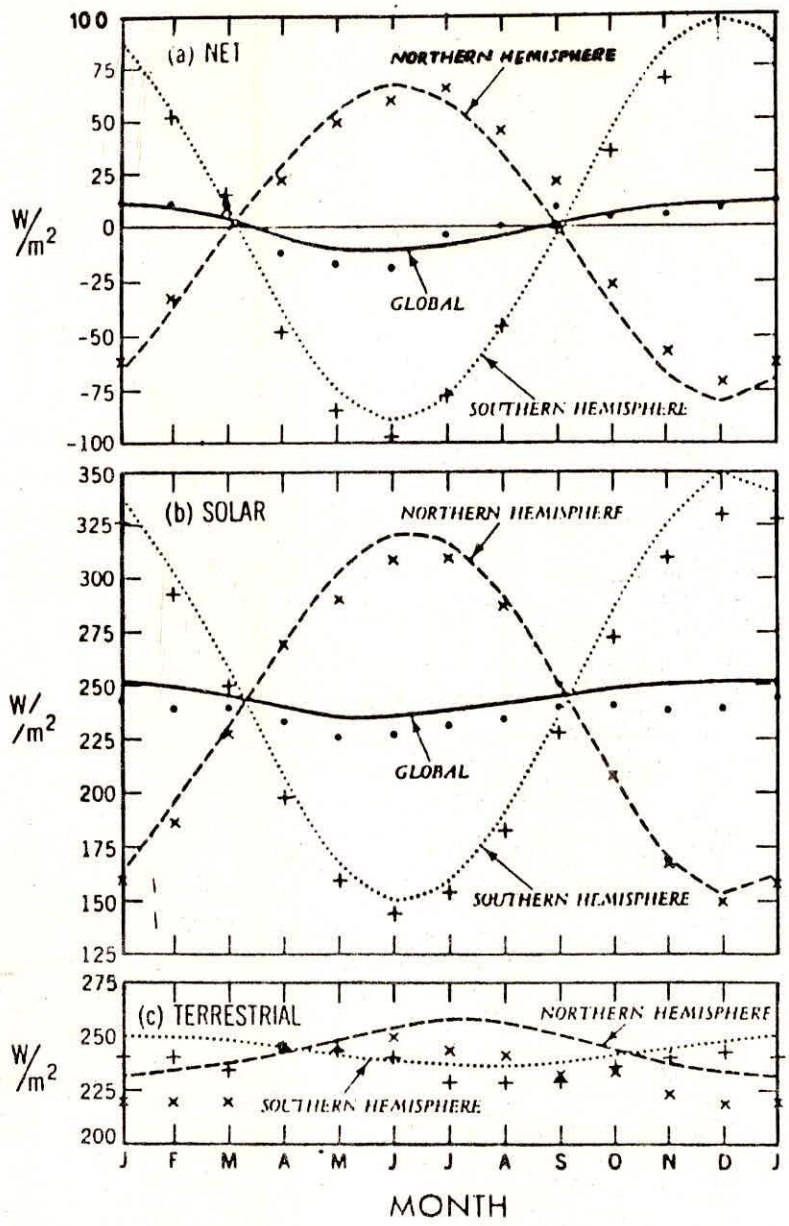

Fig. 5.4 Seasonal variations of hemispheric and global mean values of solar, terrestrial and net radiative fluxes at the top of model atmosphere. Top : net radiative flux (net downward solar flux minus upward terrestrial flux); middle: net downward solar flux (incoming solar flux minus reflected radiation); bottom : upward terrestrial flux. Units in W/m^2. Observed fluxes (crosses ,pluses and dots) from Ellis and Vonder Haar (1976)

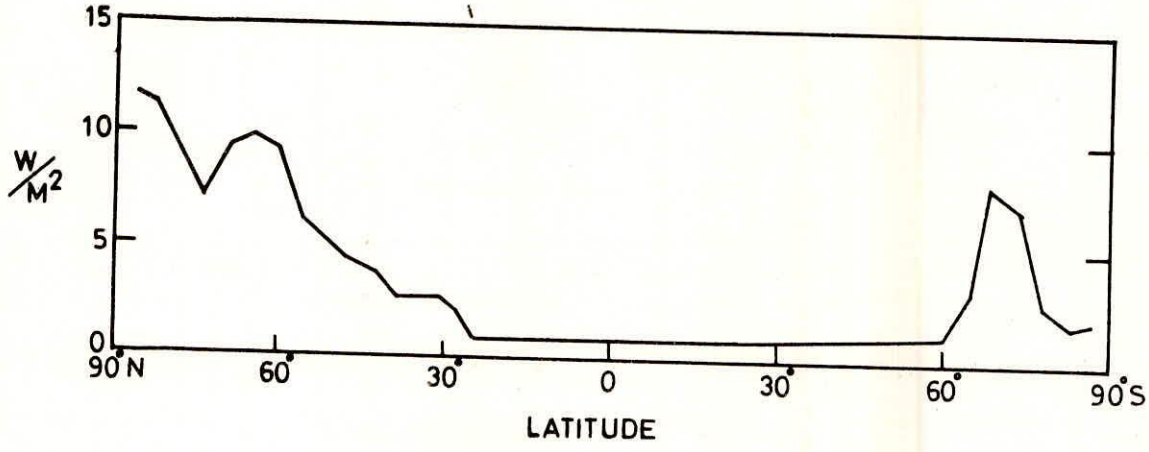

Fig. 5.5 Latitudinal distribution of the zonal mean difference in the net incoming solar radiation between $4xCO_2$ and $2xCO_2$ experiment at the top of the model atmosphere (Manabe and Stouffer, 1980)

poleward retreat of highly reflective snow cover and sea ice is significantly larger than the corresponding change in the southern hemisphere. Since the surface albedo of continents ice sheet is assumed to be almost as large as that of snow cover, the disappearance of snow cover over the Antarctic continent does not result in the significant reduction of the surface albedo and the further warming of overlying atmosphere. Thus the change of net incoming solar radiation is relatively small over the Antarctic continent despite the general warming caused by the CO_2 increase. In other words, the contribution of the snow albedo feedback mechanism is relatively small over the Antarctic continent.

Manabe and Stouffer (1980) further analyzed the zonal mean difference of various surface heat balance components - net solar radiation, net terrestrial radiation, sensible and latent heat fluxes. Fig. 5.6 shows the seasonal variation of the zonal mean differences of the these components (at $82^{o}N$) between the two experiments . A positive value in Fig. 5.6 indicates a heat gain for the ocean surface which results from the CO_2 increase. Therefore the increases in the upward fluxes of sensible heat, latent heat and net terrestrial radiation indicate negative contributions, whereas the increases in the upward oceanic heat flux and net downward solar radiation are shown to be positive contributions to the surface heat balance.

In summer, the absorption of solar radiation by the Arctic ocean surface in the $4xCO_2$ experiments is much larger than the corresponding absorption in the $1xCO_2$ experiment. The difference results from the reduction of surface albedo caused by the disappearance of sea ice or formation of water puddles over the sea ice. Figure 5.6a also indicates the net gain of terrestrial radiation energy by the Arctic ocean surface during summer. The additional energy of both solar and terrestrial radiation is transferred directly into downward oceanic heat flux and it enhances the melting of sea ice and increases the warming of mixed layer ocean. This additional heat received by the mixed layer sea ice system delays the formation of sea ice or reduces its thickness. This results in the reduction of thermal insulation effect of the sea ice in early winter, when the air sea temperature difference becomes large and enhances the warming of the surface atmospheric layer. This reduction in the thermal insulation effect of the sea ice is indicated in Figure 5.6a as a large positive difference in the oceanic heat flux around November. This change in the oceanic heat flux is accompanied by

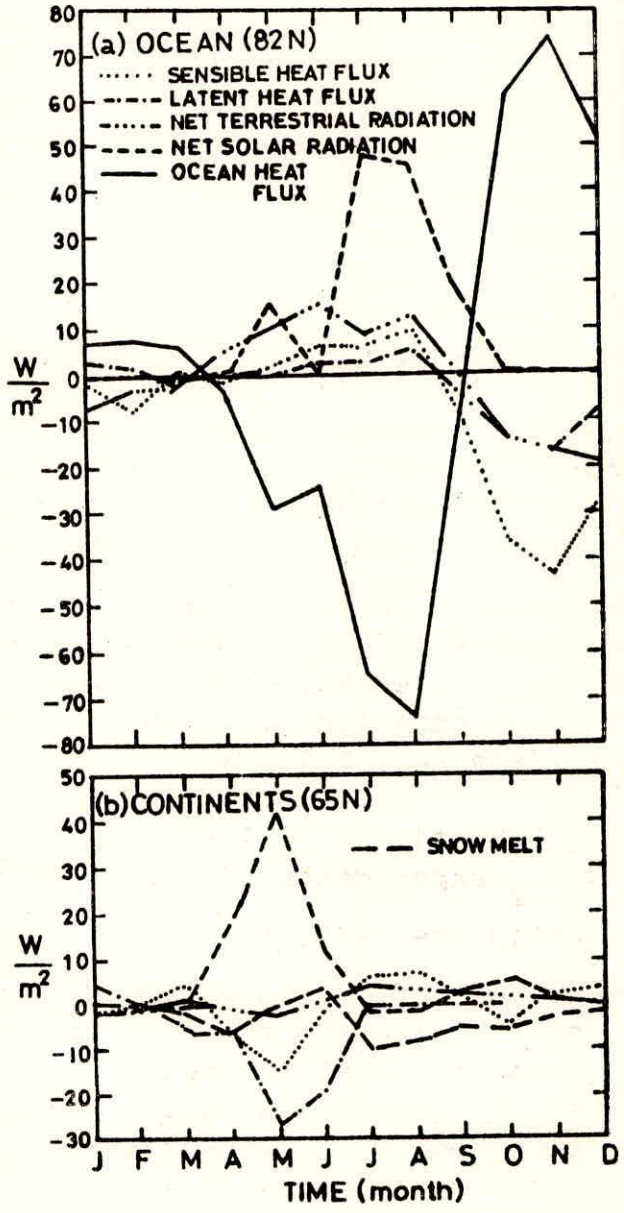

Fig. 5.6 Seasonal variation of the zonal mean differences of various balance component (Wm^{-2}) at the earth's surface between $4xCO_2$ and $2xCO_2$ experiments at (a) Ocean surface at 82°N (b) continental surface at 65°N; Units in W/m^2 (Manabe and Stouffer)

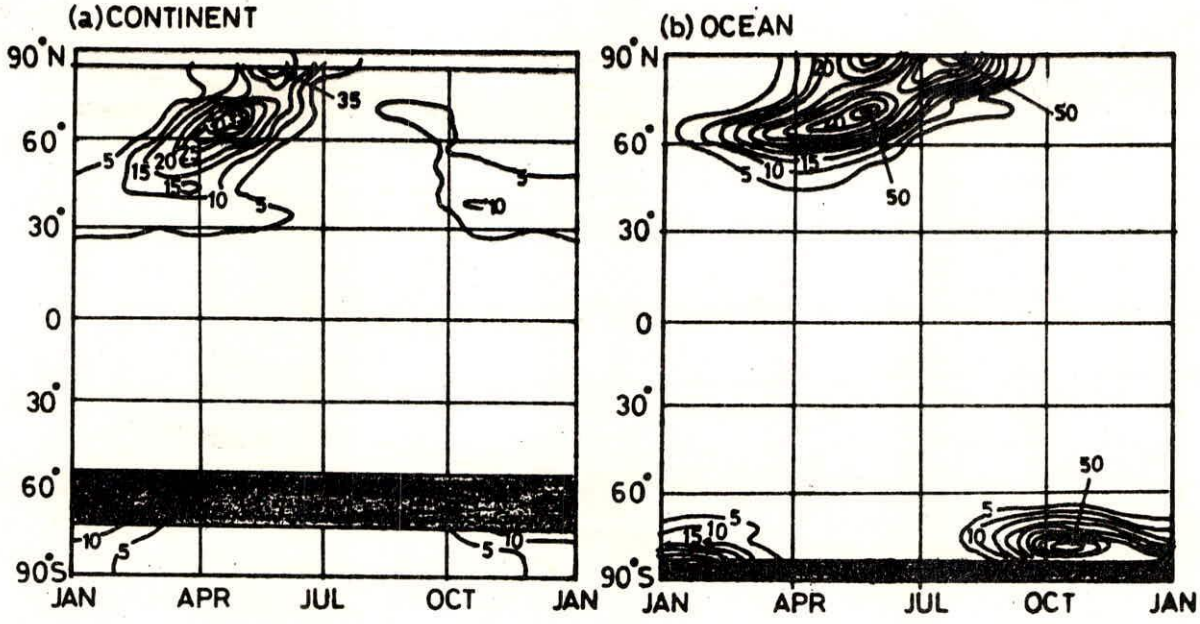

Fig. 5.7 Latitude time distribution of zonal mean difference in net incoming solar radiation (W/m^2) at top of the model atmosphere between $4xCO_2$ and $1xCO_2$ experiment (a) continents (b) oceans (Manabe and Stouffer ,1980)

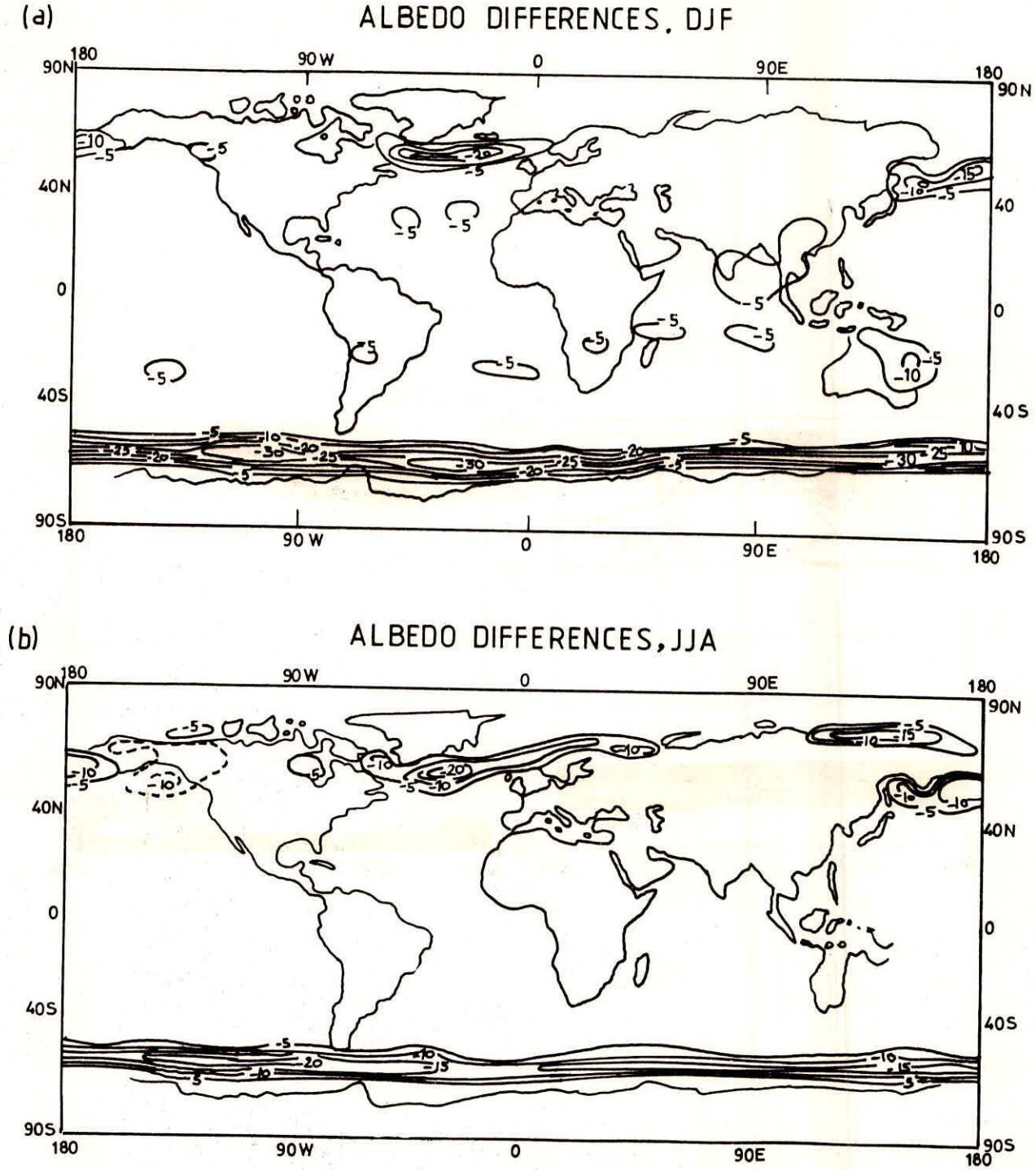

Fig. 5.8 Planetary albedo difference between $2xCO_2$ and $1xCO_2$ experiment for (a) Dec-Jan-Feb (b) Jun-Jul-Aug; contours drawn for differences greater than 5% (dashed or less than -5% (solid)(Washington and Meehl, 1984)

a large early winter increase in the sensible and latent heat fluxes into the atmosphere (a large negative difference in the sensible heat flux around November can be seen). Thus the CO_2 induced warming in the surface layer of the atmosphere is most pronounced in early winter.

Fig. 5.6b illustrates the seasonal variation of zonal mean differences of the continental heat balance components (at $65^{\circ}N$) between $4xCO_2$ and $1xCO_2$ experiments. There is a large spring maximum in the difference of net downward solar radiation between the two experiments since the incoming solar radiation of late spring is large in high latitudes, the reduction of highly reflective snow covered area in spring causes a large increase in amount of solar radiation absorbed by the continental surface. This additional solar energy immediately raises the temperature of the continental surface and is responsible for the increase in the upward fluxes of both sensible and latent heat into the model atmosphere as indicated in the Figure 5.6b by large negative differences of these fluxes around May.

It is important to note that the influence of albedo feedback mechanism upon the change in net incoming solar radiation in pronounced in the spring or early summer over the oceans as well as over the continents. This is evident in Fig. 5.7, which shows the latitude time distribution of the zonal mean difference in net incoming solar radiation at the top of the atmosphere between $4xCO_2$ and $1xCO_2$ experiments. The increase in the net incoming solar radiation over continents is most pronounced in March at around $50^{\circ}N$, in May at around $70^{\circ}N$, and in June near the North Pole. Over oceans the increase is most pronounced in the beginning of May at about $70^{\circ}N$ and in August near the North Pole. Since the high latitude insolation has pronounced seasonal variation and reaches its maximum between the spring and the summer, a change in the surface albedo because of the pole ward retreat of snow cover and sea ice results in the particularly large change in the net incoming solar radiation in these seasons.

Washington and Meehl (1984) used the NCAR atmospheric general circulation model coupled to a simple mixed layer ocean model to study the climate sensitivity due to a doubling of CO_2. They found that the largest differences in the change of planetary albedo (Fig.5.8) caused due to doubling of CO_2 occur at the ice margins as the sea ice retreat pole ward in the $2xCO_2$ experiment

(Fig.5.9).

5.2 Evaporation

Manabe and Stouffer (1980) also described the changes in the hydrologic characteristics of the model in response to the quadrupling of the CO_2 content in the atmosphere. Fig. 5.10 illustrates the latitudinal distributions of the annual mean rates of evaporation from $4xCO_2$ and $1xCO_2$ experiments. The figure reveals that the rates of evaporation increase at most latitudes in response to the quadrupling of the CO_2 concentration in the air. Manabe and Stouffer found that the global mean increase in the evaporation or precipitation rate is 0.018 cm/day which implies a 6.7% increase in the overall intensity of hydrological cycle. According to Fig. 5.10 the distribution of the CO_2 induced increase in the zonal mean rate does not have systematic latitudinal variation. The $4xCO_2$ atmosphere receives more moisture from the earth's surface in low latitudes and returns more moisture to the surface in the high latitudes than the $1xCO_2$ atmosphere.

6.0 RADIATIVE SIGNAL OF INCREASING CARBON DIOXIDE - EXPERIMENTAL APPROACH

Two viable monitoring approaches for observing the radiative signal of increasing carbon dioxide are available, to measure the spectral long wave radiance using satellite sensors (looking down from above) or to use ground based sensors (looking up from below). Both monitoring approaches have their advantages and disadvantages. Satellite sensors could provide global coverage, but calibration of the instruments is more difficult. Ground based instruments are easily serviced and could be well calibrated, but they can not easily provide global coverage. In both cases high resolution instruments would be required to measure the spectral pattern of change in radiance, which would provide important information about the cause of the change. The relative magnitude of the changes in radiance would be large in certain spectral intervals, but the change in the integrated radiance (called the flux density) would be very small at the top of the atmosphere. Although the radiative signal would be stronger at the earth's surface than in space, there would be more noise in the signal resulting from natural variability of temperature and specific humidity in the lower troposphere.

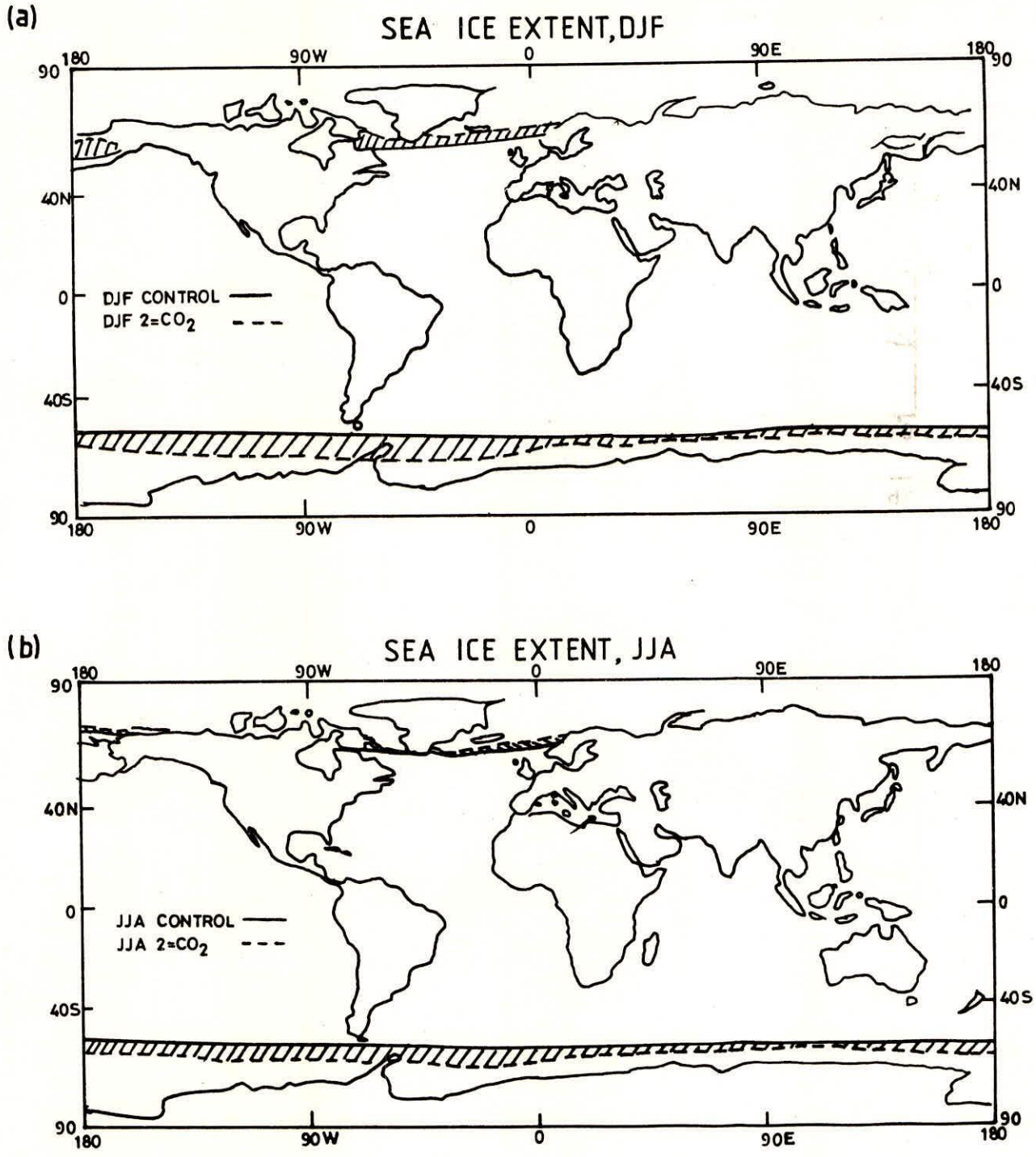

Fig. 5.9 Sea ice extent (the limit of ice 0.2 m thick) for $1xCO_2$ experiment (solid line) and the $2xCO_2$ case (dashed line). Hatching indicates areas of sea ice retreat between control and $2xCO_2$ (a) DJF, (b) JJA (Washington and Meehl ,1984)

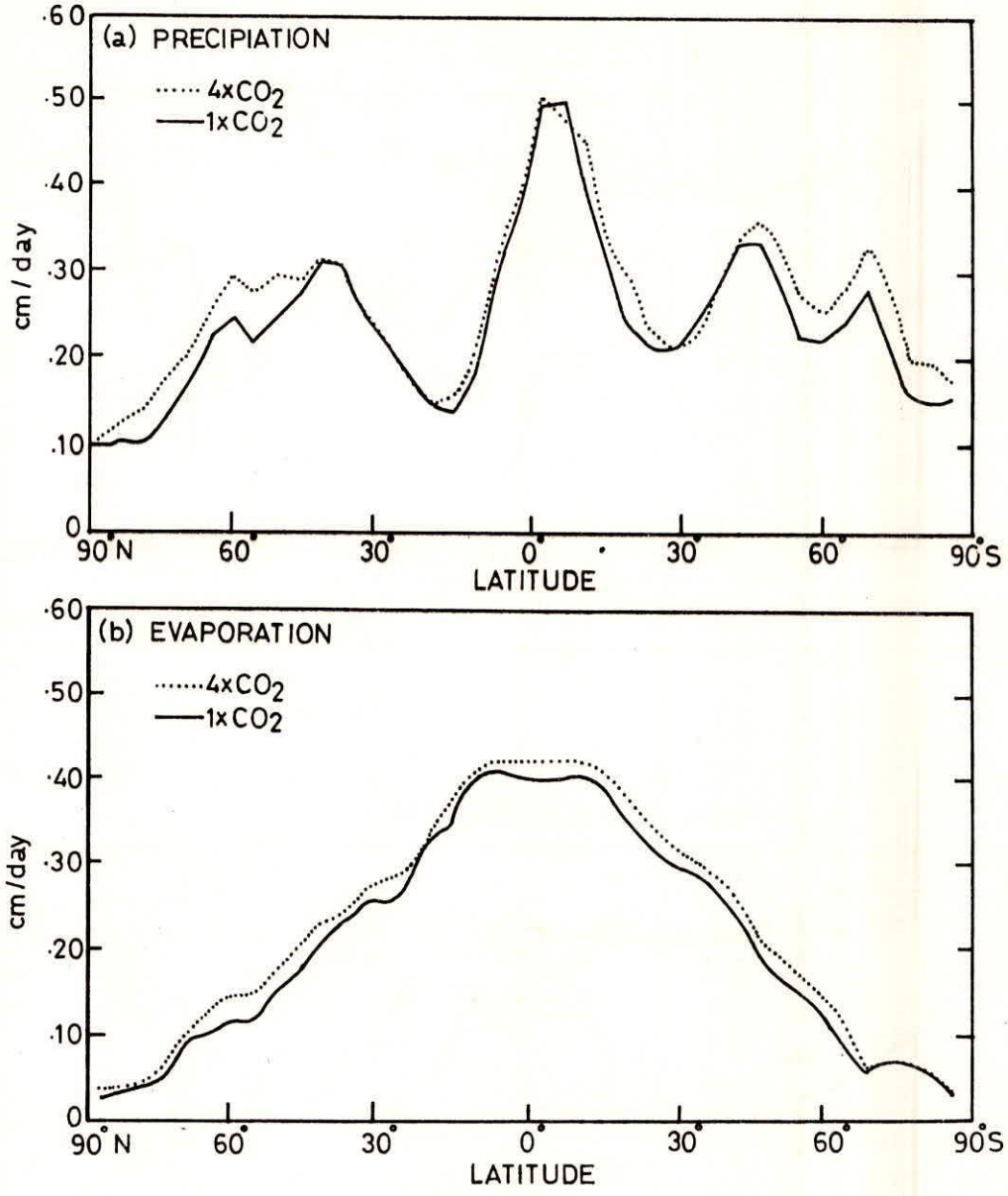

Fig. 5.10 Latitudinal distribution of (a) zonal mean precipitation rate and (b) zonal mean evaporation rate in cm/day (Washington and Meehl, 1984)

The measurement of changes in downward radiance at fixed surface locations does not appear promising in the near future as an approach for detecting CO_2 induced effects on the radiation budget. The primary uncertainty is associated with our limited understanding of the absorption and emission of energy by water vapour. Shifts in the spectral distribution of out going radiation at the top of the atmosphere measured by satellites may provide an indication that the CO_2 concentration is increasing but that is much more easily determined from ground based sampling. Satellite measurements may also indicate whether radiative fluxes to space are emanating from higher in the atmosphere, as is expected to occur as the CO_2 concentration increases. However these measurements would not provide detailed information about changes in the radiation budget of the lower atmosphere.

7.0 REMARKS

The changing concentrations of carbon dioxide and other trace gases affects the global radiation balance. The radiative perturbation changes the temperature of the surface and atmosphere, which in turn alter the wind fields and other climatic parameters and hence, hydrological parameters. Therefore as a first step, it is important to have a clear understanding of the radiation balance of the earth atmosphere system and to identify the radiative perturbation due to increase in greenhouse gases. Studies have shown that the concentration of greenhouse gases is increasing at an alarming rate.

Findings from climate models have implied that the changes in CO_2 concentrations are not expected to result in any significant change in the solar energy absorbed by the atmosphere and earth's surface. The largest changes are expected to occur in the flux density of long wave (infrared) radiation in the atmosphere. The spectral features (i.e. variations with wavelength) in the longwave flux components are affected by the particular radiative properties of CO_2, water vapour, ozone and other trace gases primarily nitrous oxide, methane and chlorofluoro carbons.

The changes in radiative fluxes due to doubling of CO_2 content also show significant latitudinal and seasonal variations. The largest changes in planetary albedo occur at the ice margins

as the sea ice retreat pole ward in the $2xCO_2$ experiment.

The alterations in net radiation at the surface would also change the evaporation from the surface, as solar energy is the driving force for phase change globally. It is likely to increase in $2xCO_2$ scenario.

In order to assess the effect of increase in greenhouse gases on radiation budget, accurate measurements of the radiative properties of trace gases are needed. Efforts must also be made to validate existing radiative transfer models against laboratory and field measurements.

REFERENCES

1. Aston A.R., 1984. The effect of doubling atmospheric CO_2 on stream flow : A simulation, J. Hydrol., 67, 273-280.

2. Aston A.R. and F.X. Dunin, 1980. The prediction of water yield from a 5 ha experimental catchment Krawarree, NSW Aust. Soil Res., 18, 149-162.

3. Augustsson T. and V. Ramanathan, 1977. A radiative convective model study of the CO_2 climate problem, J. Atmos. Sci., 34, 448-451.

4. Bultot F., G.L. Dupriez and D. Gellens, 1988. Estimated annual regime of energy balance components, evapotranspiration and soil moisture for a drainage basin in the case of a CO_2 doubling, Climatic Change, 12, 39-56.

5. Charney, J.G., 1975. Dynamics of deserts and drought in the Sahel, Q. J. Royal Meteorol. Soc., 101, 193-202.

6. Charney J.G., W.J. Quirk, S. Chow and J. Kornfield, 1977. A comparative study of the effects of albedo change on drought in semi-arid regions, J. Atmos. Sci., 34, 1366-1385.

7. Chervin R.M., 1979. Response of the NCAR atmospheric general circulation model to changed albedo, in report of the JOC study conference on climate models: Performance, intercomparison and sensitivity studies (GARP Publication Series No.22), WMO, 563-581.

8. Chou M.D., L. Peng and A Arking, 1982. Climate studies with a multi layer energy balance model. Part II: The role of feedback mechanisms in the CO_2 problem, J. Atmos. sci., 39, 2657-2666.

9. Ellis J.S. and T.H. Vonder Haar, 1976. Zonal average earth radiation budget measurement from satellite for climate studies, Atmos Sci. Pap. 240, Colo. State Univ., Fort Collins, CO.

10. Ellsaesser H.W., M.C. MacCracken, G.L. Potter and F.M. Luther, 1976. An additional model test of positive feedback

from high desert albedo, Q. J. Roy. Met. Soc., 102, 655-666.

11. Gleick P.H., 1987. The development and testing of a water balance model for climate impact assessment : modelling the Sacramento basin, Water Resources Research, 23, 1049-1061.

12. Hansen J.E., P.Lee. D. Rind and G. Russell, 1981. Climate impact of increasing atmospheric CO_2, Science, 213, 957-966.

13. Idso S.B. and A.J. Brazel, 1984. Rising atmospheric carbon dioxide concentration may increase stream flow, Nature, 312, 51-53.

14. IPCC, 1990. Climate change - The IPCC scientific assessment, Houston J.T., G.J. Jenkins and J.J. Ephraums (eds.), WMO/UNEP, Cambridge Univ. Press, USA.

15. Kiehl J.T. and V.Ramanathan, 1982. Radiative heating due to increased CO_2: The role of H_2O continuum absorption in the 12-18 μm region, J. Atmos. Sci., 39, 2923-2926.

16. Kukla G. and D. Robinson, 1980. Annual cycle of surface albedo, Mon. Wea. Rev., 108, 56-68.

17. Luther F.M. and R.G. Ellingson, 1985. Carbondioxide and the radiation budget, in Projecting the climatic effects of increasing carbondioxide, DOE/ER-0237, Washington DC 20545.

18. Manabe S. and R.F. Strickler, 1964. Thermal equilibrium of the atmosphere with a convective adjustment, J. Atmos. Sci., 21, 361-385.

19. Manabe S. and R.J. Stouffer, 1980. Sensitivity of a global climate model to an increase of CO_2 concentration in the atmosphere, J. Geophys. Res., 85, No. C10, 5529-5554.

20. Martin P., N.J. Rosenberg and M.S. Mc. Kenney, 1989. Sensitivity of evapotranspiration in a wheat field, a forest and a grassland to changes in climate and direct effects of carbon dioxide, Climatic Change, 14, 117-151.

21. Revelle R.R. and P.E. Waggoner, 1983. Effects of a carbon dioxide induced climatic change on water supplies in thee western United States, In changing climate, Nat. Acad.

Press., Washington DC, 419-432.432.

22. Ramanathan V., 1981. The role of ocean-atmosphere interactions in the CO_2 climate problem, J. Atmos. Sci., 38, 918-930.

23. Ramanathan V., M.S. Lian and R.D. Cess, 1979. Increased atmospheric CO_2: zonal and seasonal estimates of the effect on the radiation energy balance and surface temperature, J.Geophys. Res. 84, 4949-4958.

24. Wang W.C. and P.B.Ryan, 1983. Overlapping effects of atmospheric H_2O, CO_2 and O_3 on the CO_2 radiative effect, Tellus, 35B, 81-91.

25. Washington W.M. and G.A. Meehl, 1984. Seasonal cycle experiment on the climate sensitivity due to a doubling of CO_2 with an atmospheric general circulation model coupled to a simple mixed layer ocean model, J. Geophys. Res., 89, No. D6, 9475-9503.

DIRECTOR	.....	SATISH CHANDRA
TECHNICAL CO-ORDINATOR	.....	S M SETH
SCIENTIST	.....	DIVYA
OFFICE STAFF	.....	RAJNEESH KUMAR GOYAL